J Neurophysiol 90: 1095–1114, 2003.
First published March 20, 2003; 10.1152/jn.00618.2002.

Modulation of Striatal Single Units by Expected Reward: A Spiny Neuron Model Displaying Dopamine-Induced Bistability

Aaron J. Gruber,[1,2] Sara A. Solla,[2,3] D. James Surmeier,[2] and James C. Houk[1,2]
Departments of [1]Biomedical Engineering, [2]Physiology, and [3]Physics and Astronomy, Northwestern University Medical School, Chicago, Illinois 60611

Submitted 31 July 2002; accepted in final form 15 March 2003

Gruber, Aaron J., Sara A. Solla, D. James Surmeier, and James C. Houk. Modulation of striatal single units by expected reward: a spiny neuron model displaying dopamine-induced bistability. *J Neurophysiol* 90: 1095–1114, 2003. First published March 20, 2003; 10.1152/jn.00618.2002. Single-unit activity in the neostriatum of awake monkeys shows a marked dependence on expected reward. Responses to visual cues differ when animals expect primary reinforcements, such as juice rewards, in comparison to secondary reinforcements, such as tones. The mechanism of this reward-dependent modulation has not been established experimentally. To assess the hypothesis that direct neuromodulatory effects of dopamine on spiny neurons can account for this modulation, we develop a computational model based on simplified representations of key ionic currents and their modulation by D1 dopamine receptor activation. This minimal model can be analyzed in detail. We find that D1-mediated increases of inward rectifying potassium and L-type calcium currents cause a bifurcation: the native up/down state behavior of the spiny neuron model becomes truly bistable, which modulates the peak firing rate and the duration of the up state and introduces a dependence of the response on the past state history. These generic consequences of dopamine neuromodulation through bistability can account for both reward-dependent enhancement and suppression of spiny neuron single-unit responses to visual cues. We validate the model by simulating responses to visual targets in a memory-guided saccade task; our results are in close agreement with the main features of the experimental data. Our model provides a conceptual framework for understanding the functional significance of the short-term neuromodulatory actions of dopamine on signal processing in the striatum.

INTRODUCTION

The classic notion of the basal ganglia as being involved in purely motor processing has expanded over the years to include sensory and cognitive functions (Brown et al. 1997). This view is substantiated by single-unit recordings in the neostriatum, an input structure of the basal ganglia, that reveal a wide range of neural activity associated with sensory stimuli, with motor planning as well as execution, and with working memory and other cognitive functions (Schultz et al. 1995). A surprising new finding is that much of this activity shows a motivational component. For instance, neostriatal activity related to visual stimuli (Kawagoe et al. 1998) or movement planning (Hollerman et al. 1998) is dependent on the expected reinforcement a behavior will elicit. Task-related activity can be enhanced or suppressed when a reward is anticipated for correct performance. The effect of reward expectation is significant. Most task-related units show a dependence on the type of reinforcement (Hollerman et al. 1998), and the response modulation is often large enough to be clearly seen in individual trial records (Kawagoe et al. 1998). While the reward-dependent activity may have cortical origins in part (Wilson 1990), the neostriatum receives a prominent neuromodulatory signal with properties that seem quite appropriate for mediating reward dependence.

Substantia nigra pars compacta (SNpc) neurons, which send a dopaminergic input to striatal spiny neurons, discharge in a reward-dependent manner (Schultz 1998). These dopamine neurons respond not only to the delivery of unexpected rewards but also to sensory cues that reliably precede the delivery of expected rewards (Ljungberg et al. 1991; Mirenowicz and Schultz 1994; Schultz et al. 1993). The data also suggest that the responses of dopamine neurons occur at approximately the same time as striatal spiny neuron responses to visual targets (Hollerman et al. 1998; Kawagoe et al. 1998). This, in conjunction with the demonstration of dopamine-mediated neuromodulation of spiny neuron activity in vivo (Gonon 1997; Kiyatkin and Rebec 1996) and in vitro (Akaike et al. 1987; Calabresi et al. 1987; Flores-Hernandez et al. 2000; Hernandez-Lopez et al. 1997; Surmeier et al. 1992a), suggests that the release of dopamine in the neostriatum could be responsible for the reward dependence of neostriatal neurons. Nevertheless, the functional effects of dopamine on the electrophysiological properties of spiny neurons remain to be fully elucidated.

Dopamine can alter the responsiveness of medium spiny neurons through the modulation of synaptic efficacy or through the modulation of voltage-dependent ionic currents that govern the response to synaptic inputs (Nicola et al. 2000). The model presented here focuses exclusively on the latter modulatory effects of dopamine, which should accompany burst activity of SNpc neurons. These effects cannot be viewed as simply excitatory or inhibitory. For example, activation of the D1 type dopamine receptors alone can either enhance or suppress responses of spiny neurons depending on the prior state of the neuron (Hernandez-Lopez et al. 1997). This state dependence arises from the coordinated modulation of ion channels regulating these states (Flores-Hernandez et al. 2000; Hernandez-Lopez et al. 1997; Pacheco-Cano et al. 1996; Surmeier et al. 1992a, 1995). Here, we use a computational approach to assess

Address for reprint requests: J. C. Houk, Dept. of Physiology, Northwestern University Medical School, Ward 5-150, 303 E. Chicago Ave., Chicago, IL 60611 (E-mail address: j-houk@northwestern.edu).

The costs of publication of this article were defrayed in part by the payment of page charges. The article must therefore be hereby marked "*advertisement*" in accordance with 18 U.S.C. Section 1734 solely to indicate this fact.

the hypothesis that the modulation of two channel types resulting from the activation of D1 receptors is sufficient to explain both enhanced and suppressed single-unit responses of medium spiny neurons to reward-predicting stimuli.

Our goal is to construct a minimal biophysically grounded model of spiny neurons whose simplicity allows us to perform a detailed analysis of D1 receptor-mediated modulation of the model response properties and to extract from this analysis qualitative features that explain the reward dependence of neostriatal single-unit responses. We validate the model by simulating responses to visual targets in the memory-guided saccade task described by Kawagoe and colleagues (1998) and by comparing our results to the main features of their experimental data. In any given block of trials, these investigators selectively rewarded saccades made to only one of four potential targets. This allowed them to compare the response of a specific unit to a given target in rewarded as opposed to unrewarded cases. For many cells, there was a substantial reward-dependent difference. The majority of these neurons showed a reward-related enhancement of the intensity and duration of discharge, and a smaller number exhibited a reward-related depression. Dopamine neurons in the SNpc are known to have a selective response to the presentation of visual targets that precede reward in a learned task (Ljungberg et al. 1991; Schultz et al. 1993). Correspondingly, Kawagoe and colleagues (1998) suggested, and later confirmed (Kawagoe et al. 1999), that the presentation of the target in the rewarded trials serves as the conditioned stimulus that elicits SNpc discharge, which should then release dopamine in the striatum. They speculated that D1 receptor activation might explain enhanced responses, whereas D2 receptor activation might explain depressed responses. The model presented here confirms that realistic biophysical assumptions about the neuromodulatory effects of dopamine acting through D1 receptors account well for the reward-dependent enhancement of striatal unit discharge. Furthermore, due to the emergence of bistable responsiveness, D1 effects also account well for the depressed responses. Bistability constitutes a qualitative change in response characteristics, and its emergence in spiny neurons could be a very important consequence of dopamine neuromodulation.

METHODS

Model description

As stated in the INTRODUCTION, our goal is to construct a biophysically grounded membrane model that includes sufficient detail to reproduce the qualitative effects of D1 receptor activation on the characteristic up/down state behavior of spiny neurons, while remaining simple enough for detailed analysis and for inclusion in future network simulations. A detailed investigation of the static and dynamic properties of the membrane model in high and low dopamine conditions reveals generic features of reward dependence. A specific simulation illustrates the modulation of the response to target presentation for comparison to reward-dependent single-unit activity in the visually guided saccade task.

The membrane properties of the model spiny neuron result from a biophysically grounded representation of a minimal set of currents needed to reproduce the characteristic up/down state behavior of spiny neurons. These cells exhibit pseudo two-state behavior in vivo; they spend most of their time either in a hyperpolarized "down" state around –85 mV or in a depolarized "up" state around –55 mV (Wilson 1993; Wilson and Kawaguchi 1996). This bimodal character of the response to cortical input has been attributed to a combination of inward rectifying and outward rectifying potassium currents (Nisenbaum and Wilson 1995; Wilson and Kawaguchi 1996). The inward rectifying current, predominantly of the Kir2 type in spiny neurons (Mermelstein et al. 1998), contributes a small outward current at hyperpolarized membrane potentials above the K^+ equilibrium potential, thus providing resistance to depolarization and stabilizing the down state. This current accounts for most of the ionic current near the resting potential and is blocked on depolarization (Nisenbaum and Wilson 1995). The enhancement of Kir2 currents by D1 agonists is thought to be an important component of the suppressive effects of D1 activation at subthreshold potentials (Pacheco-Cano et al. 1996). The outward rectifying K^+ current in spiny neurons includes slowly and rapidly inactivating components (Nisenbaum et al. 1996; Surmeier et al. 1991, 1992b) that are attributable to different channel types. The rapidly inactivating K^+ components inactivate after the transition to the up state; it is the slowly inactivating component that influences the membrane potential for the remaining duration of the up-state episode. This current becomes activated at subthreshold potentials and opposes the depolarizing influences of excitatory synaptic and inward ionic currents; it is the balance between these inputs that determines the membrane potential of the up state. The two K^+ currents included in our model, Kir2 and Ksi (si, slowly inactivating), have been shown (Nisenbaum and Wilson 1995) to account for the characteristic nonlinear voltage dependence of the outward current measured in spiny neurons. We recognize that the si K^+ current is likely to arise from at least two channel types, but for the sake of simplicity we have treated it as a single conductance. This combined outward current acts in opposition to inward ionic and synaptic currents to regulate membrane potential in the up/down states.

The other major ionic mechanism included in the model provides an inward, depolarizing drive. L-type calcium currents are found in all medium spiny neurons (Bargas et al. 1994; Song and Surmeier 1996). In contrast to a number of other cell types, L-type currents in medium spiny neurons begin to activate at subthreshold membrane potentials, thus modulating the voltage range of the up state (Bargas et al. 1994). This subthreshold activation is attributable to the expression of Cav1.3 L-type channels by medium spiny neurons (Olson and Surmeier 2002). This current is enhanced by D1 agonists in medium spiny neurons expressing D1 receptors (Surmeier et al. 1995, 1996), and this modulation is critical to the increased excitability produced by D1 agonists at depolarized membrane potentials (Cooper and White 2000; Hernandez-Lopez et al. 1997); it is therefore included in the model.

Our approach (Gruber and Houk 2000) is to design a model that provides a consistent description of membrane properties in the 100 to 1,000 ms time range. This is the characteristic range of duration for up- and down-state episodes; it also spans the time course of short-term modulatory effects of dopamine. To provide a reliable description of the dynamical properties of spiny neurons in this intermediate time range, the model is constructed according to the principle of "separation of time scales" (Bender and Orszag 1978; Rinzel and Ermentrout 1989), a successful and fundamental technique in the study of dynamical systems. Processes that operate in the 100 to 1,000 ms range are modeled as accurately as possible. Processes that activate on a much shorter time scale are assumed to have instantaneously achieved their steady-state values. Similarly, processes that inactivate on such short time scales are not included. The time variation of processes that occur over longer time scales, such as slow inactivation, is neglected. The model therefore cannot provide a good description of rapid events such as the generation of action potentials or the precise time course of transitions between up and down states. This approach excludes many currents that contribute to the control of the membrane potential. The addition of such currents would improve the ability of the model to provide quantitative descriptions of short-term phenomena to relate to dynamical biophysical data accounted for in other models (Kitano et al. 2002; Wickens and Arbuthnott 1993), but it would not improve the usefulness of our model for determining if the enhancement of Kir2 and L-type Ca currents is sufficient to account

for the reward dependence of single-unit activity. A reliable answer to this question follows from the type of detailed analysis that can only be performed on a simple model such as the one proposed here.

In addition to a detailed analysis of the generic features of the membrane model in high and low dopamine conditions, we provide a simulation of responses to target presentation in the memory-guided saccade task used by Kawagoe and colleagues (1998). This simulation demonstrates one specific instance of the generic properties of the model for particular values of input magnitudes and duration, chosen to illustrate that response modulation accounts for the qualitative features of reward-dependent single-unit responses. The input parameters are chosen so as to be consistent with experimental data from various sources but do not impact the generic properties of the membrane model.

The components of the model used for the simulation of the saccade task are shown schematically in Fig. 1. The model spiny neuron (components inside the dashed box) receives two types of input: excitatory input from cortex and modulatory input from SNpc. Neurons in cortical regions that provide input to spiny neurons (Kemp 1970; Selemon 1985) respond phasically to sensory stimuli such as visual cue onset (Colby et al. 1996; Funahashi et al. 1990) and exhibit context-dependent tonic activity (Watanabe et al. 2002). This input is excitatory (Kitai 1976) and is modeled here through the increase of a depolarizing current conductance g_s. The model also incorporates short-term modulatory actions of dopamine release resulting from the phasic activation of SNpc neurons triggered by the detection of reward-conditioned stimuli. The short-term effects of elevated dopamine concentration on the membrane conductances of spiny neurons, represented by the neuromodulatory factor μ in Fig. 1, is not direct but is mediated through D1 receptor activation (Pacheco-Cano et al. 1996; Surmeier et al. 1995). The specification of the magnitude and time course of μ is based on an attempt to extract a coherent description from a variety of ambiguous and at times controversial biophysical and single-unit data. In this attempt, we relied more heavily on data from experiments that explore the time scales relevant to the saccade task and to processes that are likely to take place in behaving animals.

The output of the spiny neuron model in Fig. 1 is a firing rate r that is needed only to construct rasters for comparison with single-unit data. For this purpose, we obtain r from an interspike interval chosen to be a deterministic nonlinear function of the membrane potential.

Model formulation

The membrane of a spiny neuron is modeled here as a single compartment with active ion currents. A first-order differential equation relates the temporal change in membrane potential (V_m) to the membrane currents (I_i)

$$-C_m \frac{dV_m}{dt} = \mu(I_{Kir2} + I_{L-Ca}) + I_{Ksi} + I_L + I_s \quad (1)$$

The right-hand side of the equation includes active ionic, leakage, and synaptic currents; μ is the neuromodulatory factor.

TABLE 1. *Model parameters*

Parameter	Value
C_m, μF/cm^2	1
E_K, mV	−90
E_s, mV	0
g_L, mS/cm^2	0.008
Kir2 (Mermelstien et al. 1998)	
V_h^{Kir2}, mV	−111
V_c^{Kir2}, mV	−11
$\bar{g}_{Kir2}$, mS/cm^2	1.2
Ksi (Niesenbaum et al. 1996)	
V_h^{Ksi}, mV	−13.5
V_c^{Ksi}, mV	11.8
$\bar{g}_{Ksi}$, mS/cm^2	0.45
L-Ca (Bargas et al. 1994)	
V_h^{L-Ca}, mV	−35
V_c^{L-Ca}, mV	6.1
$\bar{P}_{L-Ca}$, nm/s	4.2
$[Ca]_o$, μmol/cm^3	2
$[Ca]_i$, pmol/cm^3	10
Firing model	
V_h^f, mV	−55
V_c^f, mV	2.5
V_f, mV	−58

We use a standard formulation to model the ionic currents based on parameter data obtained from the biophysical literature. The biophysical characterization of ionic currents is often done in conditions that deviate from the in vivo environment so as to facilitate data collection. Experimental conditions typically involve blocking agents, ion substitutions, and altered extracellular ionic concentrations to distinguish currents of interest. These techniques can modify the ionic current profiles away from their in vivo manifestations. Adjustments were therefore made to the parameters reported in the literature to compensate for the specific experimental conditions used in characterizing the currents. This procedure led to model currents that more closely match in vivo realizations. The parameters used in our model are listed in Table 1. The compensatory adjustments are described as specific parameters are introduced in the following description of the corresponding model currents. *Eq. 1* is integrated numerically using a fifth-order Runge-Kutta method with a 0.5-ms time step and an error tolerance of 0.1 mV/ms to determine the dynamical evolution of V_m as the inputs to the model are varied.

All currents except for L-type Ca are modeled by the product of a conductance and a linear driving force

$$I_i = g_i(V_m - E_i) \quad (2)$$

The reversal potential of ion species i is indicated as E_i; these parameters are set at biologically plausible values. The reversal potential for potassium E_K is used for all potassium currents and the leak

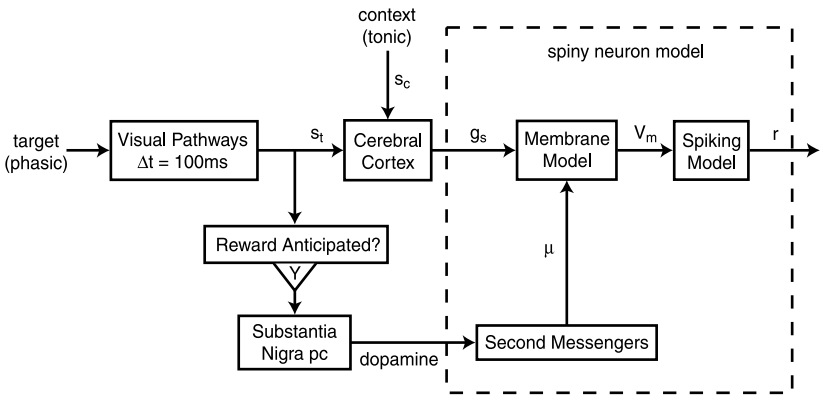

FIG. 1. Schematic diagram of the two input pathways to the model spiny neuron (components inside the dashed box): cortico- and nigro-striatal. The cortical input is composed of a tonic context-related component s_c and a phasic target-related component s_t that is activated by the target onset. It provides excitatory input to the spiny neuron by increasing a depolarizing current conductance g_s in the membrane model. The dopamine input from the substantia nigra activates if a reward is anticipated as a result of target onset and acts through a second-messenger system to control the neuromodulatory factor μ. The cortical and nigral inputs alter the membrane model properties to influence the membrane potential V_m. The output of the model is a spike train r generated as a deterministic function of V_m. A time delay Δt is associated with signal conduction through the visual pathways.

current. The factor g_i represents the conductance for ionic current type *i*. The leakage conductance is constant. The conductances for Kir2 and Ksi are voltage dependent

$$g_i = \bar{g}_i L_i(V_m) \tag{3}$$

where $\bar{g}_i$ is the maximum conductance and L_i (V_m) is a logistic function of the membrane potential

$$L_i(V_m) = \frac{1}{1 + \exp\left(-\frac{V_m - V_h^i}{V_c^i}\right)} \tag{4}$$

L varies smoothly between 0 and 1. The half activation parameter V_h determines the value of V_m at which $L = 1/2$, while V_c controls the slope of the curve. The parameters that define the conductance function for Kir2 are derived from experiments by Mermelstein and colleges (1998). These experiments were performed at $E_K = -50$ mV. The half activation parameter for Kir2 (V_h^{Kir2}) derived from their data is shifted by -40 mV for consistency with the value of $E_K = -90$ mV used in our model. Parameters for Ksi follow from a least-squares fit to data in Nisenbaum et al. (1996). The maximum conductance for Ksi derived from data in their paper is increased by 40% to compensate for the effect of the potassium channel blocker used in their experiment. The relative conductance profiles ($g_i / \bar{g}_i \equiv L_i$) of Kir2 and Ksi are shown in Fig. 2*A*. Note that only the tail of the Kir2 conductance function is operational in the normal physiological range for V_m. The resulting currents are shown in Fig. 2*B*.

Calcium currents are not well represented by a linear driving force model; extremely low intracellular calcium concentrations result in a nonlinear driving force (Hille 1992). The Goldman-Hodgkin-Katz (GHK) equation accounts for this effect and is used to model L-type Ca (Bargas et al. 1994)

$$I_{L-Ca} = P_{L-Ca}\left(\frac{z^2 V_m F^2}{RT}\right)\left(\frac{[Ca]_i - [Ca]_o \exp\left(-\frac{zV_mF}{RT}\right)}{1 - \exp\left(-\frac{zV_mF}{RT}\right)}\right) \tag{5}$$

where z is the valence of the Ca^{2+} ions, F is Faraday's constant, T is the temperature, R is the gas constant, and $[Ca]_i$ and $[Ca]_o$ refer to intracellular and extracellular concentration of Ca^{2+}, respectively. The membrane permeability is voltage dependent

$$P_{L-Ca} = \bar{P}_{L-Ca} L_{L-Ca}(V_m) \tag{6}$$

where $\bar{P}_{L\text{-}Ca}$ is the maximum permeability and $L_{L\text{-}Ca}(V_m)$ is a logistic function of the membrane potential (see *Eq. 4*). Parameters for L-type Ca are obtained from Bargas et al. (1994). The parameter values derived from these experiments are adjusted to compensate for their use of Ba^{2+} in place of Ca^{2+} as the charge carrier; the amplitude of the peak current is seven times larger and the corresponding value of the potential exhibits a depolarized shift when measured at external concentrations of 10 mM Ba^{2+} as compared with 2 mM Ca^{2+} (Bargas et al. 1994) (see Fig. 4). The reported value of $P_{L\text{-}Ca}$ is accordingly reduced by a factor of 7 and $V_h^{L\text{-}Ca}$ is shifted by -24 mV to represent the properties of the L-type Ca current at 1–2 mM Ca^{2+}, which more accurately represents the in vivo environment. The resulting relative permeability for L-type Ca (Fig. 2*A*) starts to rise around -50 mV, within the physiological range for L-type Ca current activation as predicted for Cav1.3 (L-type) Ca^{2+} channels in medium spiny neurons (Olson and Surmeier 2002). The corresponding current is shown in Fig. 2*B*.

The model includes two types of excitatory input signals: context s_c and visual target s_t (see Fig. 1), which represent the collective input from many cortical neurons. The context signal is the sum of all tonic inputs representing persistent neural activity related to the environment and task expectation (Watanabe et al. 2002). The visual target signal is the sum of all phasic inputs representing a simplified version of the responses of cortical neurons to a visual cue (Colby et al. 1996). These two types of input are combined to obtain the synaptic current, which is modeled as the product of a conductance and a linear driving force, $I_s = g_s(V_m - E_s)$. The excitatory synaptic conductance is determined by the sum of the context and target input signals

$$g_s = \xi(w_c s_c + w_t s_t) = \xi(g_c + g_t) \tag{7}$$

where w_c and w_t are the synaptic efficacies that transform input signals into their corresponding synaptic conductances. Inhibition is not included in this model. The factor ξ is a random variable included to simulate the noisy character of synaptic input. The statistics of ξ are chosen so that the fluctuations of V_m in the up state have a similar amplitude and power spectrum as the high-frequency (>10 Hz) membrane potential fluctuations seen in intracellular recordings of spiny neurons (Stern et al. 1997). The synaptic input used here is more biologically relevant than the constant injected current term frequently used in computational models. An injected current independent of the membrane potential would be represented as a horizontal line in Fig. 3*A*. The absolute value of the synaptic driving force ($V_m - E_s$) used in our model decreases linearly as the membrane potential is depolarized, and becomes zero at the reversal potential $E_s = 0$ (thin lines in Fig. 3*A*). The net conductance g_s in *Eq. 7* determines the slope of the synaptic current lines in Fig. 3*A*.

Dopamine modulates the properties of ion currents through the activation of dopamine receptors. Agonists for the D1 type receptor enhance the Kir2 and L-type Ca currents observed in spiny neurons (Hernandez-Lopez et al. 1997; Pacheco-Cano et al. 1996; Surmeier et al. 1995). This effect is modeled by the neuromodulatory factor μ, which scales Kir2 and L-type Ca currents (see *Eq. 1*). An upper bound at $\mu = 1.4$ is derived from physiological experiments on the modulation of Kir2 and L-type Ca currents when D1 receptors or their effector mechanisms are activated (Surmeier et al. 1995; Surmeier, unpublished observations). The lower bound at $\mu = 1.0$ corresponds to low dopamine levels; this is the experimental condition in which the ion currents have been characterized. The assumption of $\mu = 1.0$

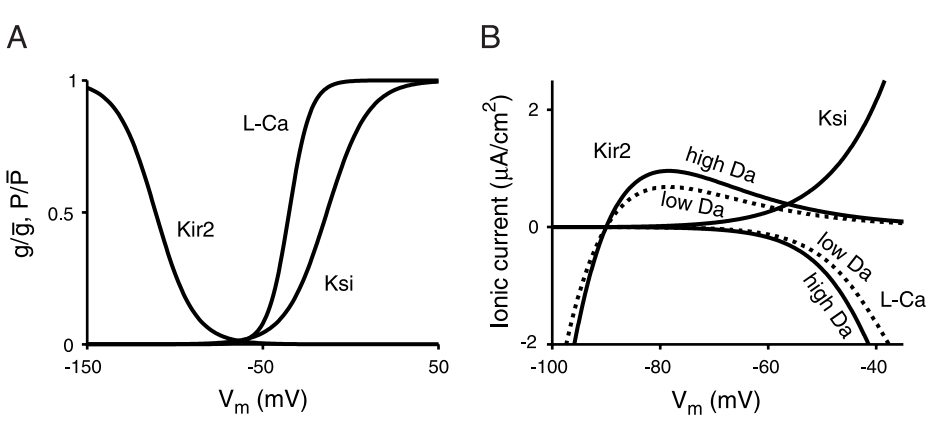

FIG. 2. Voltage dependence of relative ion conductances and permeability (*A*) and the resulting ionic currents (*B*) in high ($\mu = 1.4$; —) and low ($\mu = 1$; · · ·) dopamine conditions. The high-dopamine condition increases Kir2 and L-type Ca currents by 40%. Note that the rightward tail of the Kir2 gating function in *A* extends beyond the K^+ reversal potential (-90 mV), which causes the small inactivating outward Kir2 current seen in *B*.

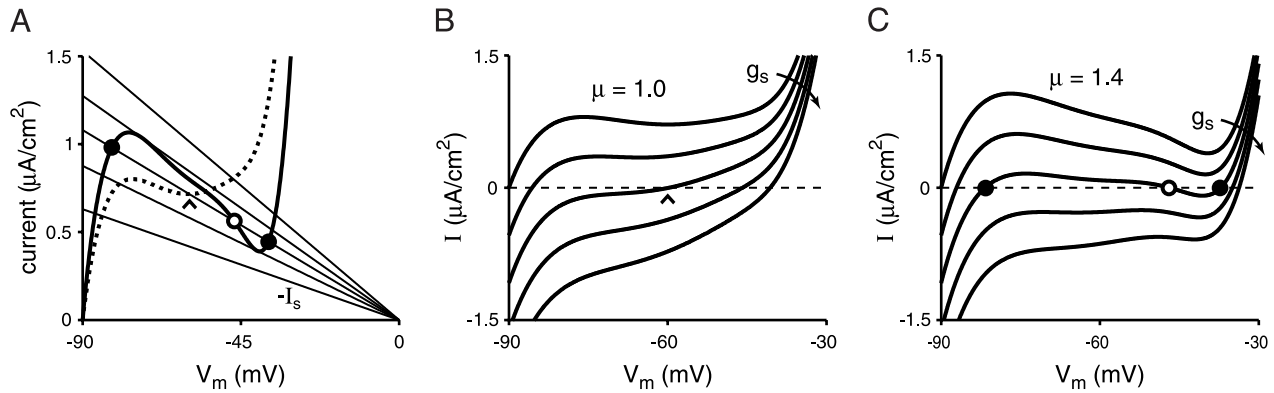

FIG. 3. *A*: intersections between the net ionic current (thick curves) and the negative of the synaptic current (thin lines) are fixed points where $dV_m/dt = 0$. The 5 thin lines in *A* correspond to $g_s = 7$, 9.74, 12, 14.17, and 17 μS/cm^2. The slope of the net ionic and synaptic currents at an intersection determine the stability of corresponding fixed point. In low dopamine conditions (A, dotted curve; $\mu = 1$), there is 1 stable fixed point for any value of g_s. The arrowhead indicates the stable solution for $g_s = 12$ μS/cm^2. In high dopamine conditions (A, solid curve; $\mu = 1.4$), there is 1 stable fixed point for $g_s < 9.74$ μS/cm^2 or $g_s > 14.17$ μS/cm^2. In the intermediate regime, there are 3 fixed points for each value of g_s. The circles show the solutions for $g_s = 12$ μS/cm^2; the outer solutions (filled circles) are stable and the intermediate solution (open circle) is unstable. Current-voltage curves for $g_s = 6$, 12, 18, and 24 μS/cm^2 at $\mu = 1$ (*B*) and $\mu = 1.4$ (*C*) illustrate the nonlinear effect of g_s on V_m. The curved arrows indicate the direction of increasing g_s. Note that although a region of negative slope conductance exists for small values of g_s at $\mu = 1$ in *B*, no bistability is present in the operational curve at $\mu = 1$ due to this nonlinear relationship.

neglects any effects of background dopamine, a reasonable approach given the low basal concentration of dopamine in the striatum (Herrera-Marschitz et al. 1996) and the predominantly low affinity of D1 receptors to the ligand (Richfield et al. 1989). The potential importance of basal dopamine levels (Grace 1991), the effect of which on ion current properties is not well characterized, is likely to manifest itself in relation to predominantly high-affinity D2 or D5 receptors not incorporated in our model.

The time course over which μ varies between the upper and lower bounds is controlled by transmitter diffusion, the rate of receptor activation, and the kinetics of the intracellular cascade that ultimately leads to the modulation of ion currents. There is insufficient data to accurately model the time course of these processes to specify $\mu(t)$ and thus describe how μ changes with time after dopamine release. To minimize the dependence of our results on an explicit form for $\mu(t)$, we first perform a detailed analysis of those generic properties of the modulation that are independent of the dynamics of μ. It is only when we come to the simulation of the saccade task that we need to chose an explicit form for $\mu(t)$ to test if the interaction between the dynamics of the inputs and the dynamics of the membrane model leads to reward-dependent responses similar to those observed in the single-unit data.

To approximate $\mu(t)$, we rely on experiments in which dopaminergic neurons are stimulated in a manner that mimics the naturally occurring bursts in response to conditioned visual stimuli (Gonon 1997). Some spontaneously active spiny neurons display an increased firing rate after evoked dopamine transients elicited through stimulation of the medial forebrain bundle (Gonon 1997). The enhancement of activity begins with a latency of 200 ms after the initiation of the stimulation and trails off up to 1,000 ms later. This latency reflects both the lag due to second messengers and the subsequent dynamical response of the membrane potential. Earlier experiments by Williams and Millar (1990) used a high stimulation frequency (50 Hz), delivering a minimum of 25 pulses, as opposed to the 1–4 pulses delivered at 15 Hz in the Gonon (1997) experiments. This more intense stimulation of the medial forebrain bundle produced responses that lasted tens of seconds, which we are presuming not to reflect naturally occurring bursts in response to conditioned visual stimuli.

The form of $\mu(t)$ we choose here is a fast exponential rise toward a maximum value beginning with a delay of 80 ms after the onset of SNpc activity, followed by a slower exponential decay to a baseline level beginning with a delay of 600 ms. The response of SNpc neurons to a visual cue follows the onset of the stimulus by ~100 ms (Schultz et al. 1993). This delay is also included in the model; the μ transient thus begins 180 ms after the onset of the visual cue. The relatively brief modulatory effects considered here are to be distinguished from longer-lasting effects observed in experiments that employ direct application of dopamine for long periods or at high concentrations (Umemiya and Raymond 1997). These long-term effects, which could be either synaptic or modulatory in nature, are not explored in the present model.

In the model described by *Eq. 1*, the membrane potential V_m is a state variable, the value of which depends on two inputs: the synaptic conductance g_s and the neuromodulatory factor μ. Although *Eq. 1* is linear in both μ and g_s, the currents at the right-hand side of the equation exhibit a significantly nonlinear dependence on V_m. Both the equilibrium and the dynamical dependences of V_m on g_s and μ are therefore nonlinear. These nonlinearities play an essential role in determining the response properties of the membrane model.

The output of the model neuron is expressed as a spike train r, which is used to construct rasters and histograms so as to allow for comparison to the neurophysiological data on single-unit response properties in the saccade task. The spike train is chosen to be a deterministic function of membrane potential and time

$$r = \begin{cases} 0 & \text{if } V_m < V_f \quad \text{or } t - t_p < (0.05 L_f(V_m))^{-1} \\ 1 & \text{otherwise} \end{cases} \tag{8}$$

where V_f is the firing threshold for generating spikes, t is the time in milliseconds, and t_p is the time at which the previous action potential occurred. In this formulation, no spike occurs if the membrane potential is below threshold or if the time $(t - t_p)$ elapsed since the last spike is less than the instantaneous interspike interval calculated as a deterministic function of V_m. When V_m is below the firing threshold, t_p is set to a small value so as to allow a spike to occur as soon as the firing threshold is exceeded. However, the interspike interval is never smaller than 20 ms even if V_m fluctuates rapidly above and below the firing threshold. V_f is set at -58 mV, consistent with experimental data (Wilson and Kawaguchi 1996); this value is slightly more depolarized than the normal up-state potential of spiny neurons. Values for V_h and V_c are chosen so that the excitatory input corresponding to target presentation results in a firing rate of 50 spikes/s in unrewarded trials, as seen in Fig. 1 of Kawagoe et al. (1998). The values of these parameters do not influence the qualitative properties of the model;

they only determine the magnitude of the response in high relative to low dopamine conditions.

RESULTS

In the ensuing section, we present a detailed analysis of the spiny neuron membrane model introduced in METHODS. This minimal model displays complex nonlinear dynamics. We begin by identifying the fixed points that characterize the stationary properties of the model; we then show that dopamine-induced bifurcations of these fixed points lead to bistability. The dynamical responses of the model first to cortical inputs and then to neuromodulatory inputs at fixed levels of cortical activity are analyzed. Finally, responses to combined cortical and neuromodulatory inputs are considered. This analysis begins with a discussion of generic features of the model's response properties, which are independent of the spiking mechanism and of the neuromodulatory dynamics. We then illustrate these features through a simulation of the saccade task that incorporates specific assumptions about the dynamics of both cortical and neuromodulatory inputs as well as the spiking mechanism. The resulting predictions for the characteristics of reward-dependent single-unit discharge are presented in the final part of this section. In the DISCUSSION, we will relate the results presented here to existing experimental data.

Fixed points and dopamine-induced bifurcations

The dynamical evolution of the membrane potential V_m is controlled by the sum of ionic and synaptic currents that appear in the right-hand side of *Eq. 1*. The stationary solutions to *Eq. 1* correspond to equilibrium values of the membrane potential V_m consistent with specific values of the dopamine-controlled neuromodulatory factor μ and the synaptic conductance g_s. Fluctuations of this conductance around its mean value $g_s = g_c + g_t$ are ignored until later by setting $\xi = 1$. The equilibrium values of V_m satisfy $dV_m/dt = 0$; it follows from *Eq. 1* that such values are the solutions to

$$\mu(I_{Kir2} + I_{L-Ca}) + I_{Ksi} + I_L = -I_s \quad (9)$$

These solutions are called *fixed points* to emphasize that such values of V_m, once attained, will not change with time. The stationary values of V_m for given values of g_s and μ remain fixed through a cancellation between the net outward ionic current and the inward synaptic current. In such a configuration, the membrane potential cannot change unless the system is perturbed.

A useful visual tool for the identification of fixed points and the analysis of their stability properties is shown in Fig. 3*A*. Although synaptic and ionic currents play a mathematically equivalent role in determining the equilibrium values of V_m, we choose to differentiate them so as to illustrate the separate dependence of the stationary properties of the model on the two parameters that determine them: μ and g_s. The sum of the ionic currents is plotted in Fig. 3*A* as a function of the membrane potential V_m for both low ($\mu = 1$, dotted curve) and high ($\mu = 1.4$, dark solid curve) dopamine levels. The shape of this relationship depends markedly on the value of μ. Note that the net ionic current is outward whenever V_m is more depolarized than the resting potential at $V_m = -89.99$ mV, which is very close to the reversal potential for potassium at $E_K = -90$mV. Synaptic current is represented in Fig. 3*A* by a family of straight lines that pivot around the reversal potential at $E_s = 0$. The increasing steepness of the lines corresponds to increasing values of g_s. Synaptic current is inward: I_s is negative, whereas the plot shows $-I_s = -g_s(V_m - E_s)$, which is positive. This separate consideration of the synaptic currents is particularly useful for the analysis of our model; as opposed to in vitro scenarios where the magnitude of injected currents is a control variable, we address the case of cortical inputs that control instead the synaptic conductance g_s.

Intersections between a curve representing the net ionic current and one of the straight lines representing the negative of the synaptic current determine the stationary values of the membrane potential, the fixed points of the model. These solutions can be followed as a function of g_s for fixed μ by varying the slope of the straight line. At low-dopamine levels ($\mu = 1$), there is only one such intersection for each value of g_s; the arrowhead in Fig. 3*A* shows this solution for $g_s = 12$ μS/cm^2. The corresponding stationary membrane potential is a single-valued function of the synaptic conductance. At high-dopamine levels ($\mu = 1.4$), the membrane potential is a single-valued function of the synaptic conductance for either $g_s < 9.74$ μS/cm^2 or $g_s > 14.17$ μS/cm^2. In contrast, there are three fixed point solutions to *Eq. 9* for each value of g_s in the intermediate regime 9.74 μS/cm^2 $< g_s <$ 14.17 μS/cm^2; the circles in Fig. 3*A* show these solutions for $g_s = 12$ μS/cm^2. This switch from single solutions to multiple solutions results in a qualitative change in the dynamical properties of the membrane model, as will be discussed in detail in the following text.

It is important to analyze the stability of fixed point solutions against perturbations. A perturbation to a stable fixed point results in a dynamical convergence back to the fixed point; a perturbation to an unstable fixed point results in a dynamical divergence away from it. For the fixed point solutions of *Eq. 1*, stability is determined by the competition between ionic and synaptic currents in the vicinity of the fixed point. The relevant comparison is between the slope of the net ionic current and the slope of the negative of the synaptic current at the intersection point; the latter is always negative and given by $-g_s$. If the slope of the net ionic current at the fixed point is greater than $-g_s$, the ionic current dominates to the right of the solution while the synaptic current dominates to the left. The total current is positive (outward) to the right of the solution, which will decrease V_m toward the fixed point; the total current is negative (inward) to the left of the solution, which will increase V_m toward the fixed point. This scenario corresponds to a stable fixed point: a perturbative depolarization (hyperpolarization) is followed by a dynamical hyperpolarization (depolarization), and the stationary state is restored. This condition is met by all fixed point solutions of *Eq. 1* for $\mu = 1$ (arrowhead in Fig. 3*A*) and by the outer solutions (filled circles in Fig. 3*A*) for $\mu = 1.4$. This condition will always be satisfied when the slope of the net ionic current at the intersection is positive; it will also be satisfied if the slope of the net ionic current at the intersection is negative but smaller in absolute value than g_s (i.e., the net ionic current is less steep than the negative of the synaptic current). The intermediate solution for $\mu = 1.4$ (open circle in Fig. 3*A*) illustrates the opposite scenario: the slope of the net ionic current at the fixed point is less than the slope of the negative of the synaptic current. In this case, the slope of the

net ionic current at the intersection is negative but larger in absolute value than g_s (i.e., the net ionic current is steeper than the negative of the synaptic current). The synaptic current dominates to the right of the solution while the ionic current dominates to the left. The total current is negative (inward) to the right of the solution, which will increase V_m further away from the fixed point; the total current is positive (outward) to the left of the solution, which will decrease V_m further away from the fixed point. A perturbative depolarization (hyperpolarization) is enhanced by a dynamical depolarization (hyperpolarization); the fixed point is unstable. Note that the boundary between stability and instability occurs where the slope of the ionic current at the fixed point is negative and equal to g_s in absolute value. For the curves shown in Fig. 3*A*, this condition is met for $g_s = 9.74\ \mu S/cm^2$ and $g_s = 14.17\ \mu S/cm^2$.

An alternative and perhaps simpler approach to the stability analysis follows directly from *Eq. 1*, which can be written as $-C_m\, dV_m/dt = I(V_m, g_s, \mu)$. The dynamical evolution of V_m is controlled by the sum $I(V_m, g_s, \mu)$ of all the currents; this total current is shown as a function of V_m for various values of g_s in Fig. 3, *B* ($\mu = 1$) and *C* ($\mu = 1.4$). Fixed point solutions to *Eq. 1* correspond to $I(V_m, g_s, \mu) = 0$ (dashed horizontal lines in Fig. 3, *B* and *C*). The stability of these solutions is controlled by the sign of the slope of the corresponding curve as it passes through $I(V_m, g_s, \mu) = 0$. A positive slope implies that dV_m/dt is negative (outward net current) to the right of the fixed point and positive (inward net current) to its left; this scenario results in negative feedback and corresponds to a stable solution. Conversely, a negative slope implies that dV_m/dt is positive (inward net current) to the right of the fixed point and negative (outward net current) to its left; this scenario results in positive feedback and corresponds to an unstable solution. Curves for $\mu = 1$ (Fig. 3*B*) exhibit a single stable fixed point for each value of g_s. Curves for $\mu = 1.4$ (Fig. 3*C*) exhibit a single stable fixed point for low and high values of g_s but three fixed points for intermediate values of g_s. As in Fig. 3*A*, the outer fixed points (filled circles) are stable, while the one in the middle (open circle) is unstable.

It is worth remarking on an interesting feature displayed by the *I-V* curves shown in Fig. 3, *B* and *C*: a region of negative slope conductance is a necessary but not a sufficient condition for instability. The *I-V* curves are N-shaped at $\mu = 1$ for low values of g_s, and yet no instability is observed at $\mu = 1$; increases in g_s do not merely shift the *I-V* curve vertically downward (as voltage-independent increases in the magnitude of an injected current would) but also affect the shape of the curves so as to gradually shrink away the range of values of V_m for which negative slope conductance is observed. The occurrence of instability at $\mu = 1.4$ is due to a persistence of this region of negative slope conductance. Both the I_{Kir2} and $I_{L\text{-}Ca}$ currents, whose conductances are enhanced by dopamine, contribute to the positive feedback associated with the existence of an unstable fixed point at voltages intermediate to those characteristic of the down and up states and thus provide a mechanism for the persistence of negative slope conductance.

Operational curves and emergence of bistability

A full characterization of the membrane model is provided by the relationship between the state variable V_m and the two input variables: the synaptic conductance g_s and the dopamine controlled neuromodulatory factor μ (Fig. 1). Treating the dependence on μ as a parameter, we can plot V_m as a function of g_s for different values of μ and use these *operational curves* to explore the consequences of neuromodulation. For low values of μ, V_m is a smooth, monotonic function of g_s. The dotted curve for $\mu = 1$ in Fig. 4*A* exhibits a steep but smooth transition from hyperpolarized values of V_m corresponding to the down state to depolarized values of V_m corresponding to the up state. The curve for $\mu = 1.4$ in Fig. 4*A* is qualitatively different; it consists of a lower branch (dark curve) corresponding to a stable hyperpolarized down state, an upper branch (dark curve) corresponding to a stable depolarized up state, and an intermediate unstable branch (gray curve) connecting these two. The resulting *bistability* for intermediate values of g_s, due to the enhancement of the Kir2 and L-type Ca ionic currents, has a drastic effect on the response properties of the model in high dopamine conditions. This qualitative change in the dy-

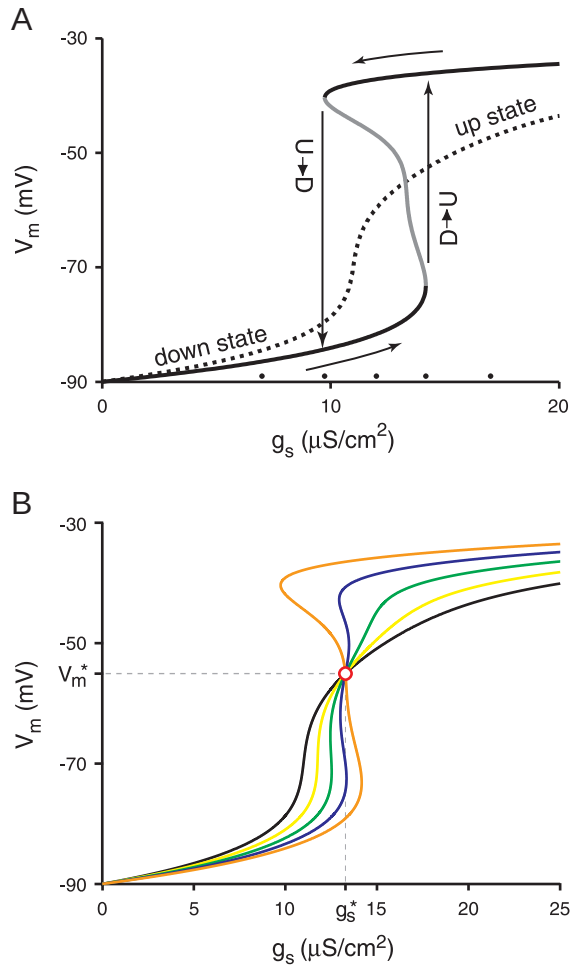

FIG. 4. *A*: the operational curve for $\mu = 1$ (dotted curve) is a single valued monotonically increasing function. The operational curve for $\mu = 1.4$ (solid curve) consists of 3 branches: 2 stable branches (black solid curves) and an unstable branch (solid gray curve). "D→ U" and "U→ D" mark the edges of the bistable region and indicate the transition thresholds to the depolarized and hyperpolarized states, respectively. Small dots along the horizontal axis identify the values of g_s used in Fig. 3*A*. *B*: operational curves for $\mu = 1.0$ (black), 1.1 (yellow), 1.2 (green), 1.3 (purple), and 1.4 (red). Note the increasing width of the bistable region in g_s for increasing μ. All lines intersect at the critical point (g_s^*, V_m^*), marked by a circle.

namical properties of the membrane model as μ increases from 1 to 1.4 is the signature of a *bifurcation*.

Consider a quasistatic experiment in which μ is fixed at 1.4 and the synaptic conductance changes slowly so that the membrane potential is allowed to reach its corresponding equilibrium value. As g_s increases, a hyperpolarized down state evolves following the lower dark solid curve in Fig. 4*A*. When g_s reaches 14.17 μS/cm^2, the synaptic current starts to overcome the mostly Kir2 hyperpolarizing current, and V_m depolarizes abruptly until it reaches the up state, which is stabilized by the hyperpolarizing Ksi current. This jump in V_m is a discontinuous change in state, the down state to up state transition (D→U) in Fig. 4*A*. If g_s is increased further, the depolarized up state follows the upper dark solid curve in Fig. 4*A*, with a small amount of additional depolarization. If g_s is now decreased, the depolarized up state will follow the upper dark solid curve in Fig. 4*A* in the downward direction. It is the enhanced effect of the inward L-type Ca current that counteracts the hyperpolarizing effect of the Ksi current and stabilizes the up state until g_s reaches 9.74 μS/cm^2. At this point, the net hyperpolarizing ionic current starts to overtake the synaptic current, and V_m hyperpolarizes abruptly until it reaches the down state. This jump in V_m is the up to down state transition (U→D) in Fig. 4*A*. Throughout the intermediate range 9.74 μS/cm^2 $< g_s <$14.17 μS/cm^2, V_m will reach either of its two stable values, depending on the previous state; this memory of prior state is called *hysteresis*.

The emergence of bistability in high dopamine conditions, characterized by the appearance of sharp and distinct state transitions, results in a prominent hysteresis effect. The state of the model, as described by the value of the membrane potential, depends not only on the current values of μ and g_s but also on the particular trajectories followed by μ and/or g_s to reach their current values. The appearance of bistability at high-dopamine levels gives additional meaning to the notion of a down state and an up state, as in this case there is a well-defined gap between the two stable branches (dark solid curves in Fig. 4*A*) that characterize the membrane potential. There is a maximal value of V_m for the lower branch; this is the most depolarized potential attainable in the down state. The minimal value of V_m in the upper branch is the most hyperpolarized potential attainable in the up state. Intermediate values of V_m correspond to the unstable branch (solid gray curve) in Fig. 4*A*. The model cannot sustain membrane potentials in this range without an external driving force such as could be provided through voltage clamp. In contrast to this sharp separation, the transition between down and up states in low dopamine conditions (dotted curve in Fig. 4*A*) is smooth with no clear separation between them. We will nevertheless refer to hyperpolarized potentials as the down state and depolarized potentials as the up state for consistency with the terminology conventionally used in the description of spiny neuron electrophysiology (Wilson and Groves 1981; Wilson and Kawaguchi 1996).

Bistability in high dopamine conditions arises in this model through a saddle-node bifurcation with increasing μ. To investigate the bifurcation, it is useful to consider a family of operational curves for subsequent values of μ, as shown in Fig. 4*B* for $\mu = 1.0$, 1.1, 1.2, 1.3, and 1.4. Curves for $\mu = 1.0$ and $\mu = 1.1$ follow a single stable solution for which V_m is a smooth, monotonically increasing function of g_s. The curve for $\mu = 1.2$ displays an unstable branch for -71.4 mV $< V_m <$ -65.4 mV; this instability at hyperpolarized potentials is due primarily due to the enhancement of the Kir2 current. The resulting hysteresis loop is extremely narrow: it corresponds to a change of $\Delta g_s \cong 0.07$ μS/cm^2 in synaptic conductance. The "double S" shape of the curve for $\mu = 1.3$ reflects the existence of two unstable branches separated by an additional intermediate stable branch; this type of operational curve results in two distinct ranges of unstable values for V_m. The associated hysteresis loop is still narrow: it corresponds to a change of $\Delta g_s \cong$ 0.54 μS/cm^2 in synaptic conductance. These narrow hysteresis loops are to be contrasted with the one observed for $\mu = 1.4$, characterized by a change of $\Delta g_s \cong 4.43$ μS/cm^2 in synaptic conductance. It is at this higher value of μ, of relevance to our model, that bistability is present for a significantly wide range of synaptic inputs and thus plays an important role in determining the dynamical properties of the membrane model.

A remarkable feature of Fig. 4*B* is that curves for all values of μ intersect at a unique point, at which $V_m^* = -55.1$ mV and $g_s^* = 13.28$ μS/cm^2. The existence of this *critical point* is due to a cancellation between the Kir2 and the L-type Ca currents for this particular value of V_m, which arises as a solution to the equation

$$I_{Kir2} + I_{L-Ca} = 0 \qquad (10)$$

When this condition is satisfied, solutions to *Eq. 9* become independent of μ; for $g_s = g_s^*$, a change in μ does not result in a corresponding change in the equilibrium value of the membrane potential.

The location of this critical point follows from the model formulation of the Kir2 and the L-type Ca currents; the value of V_m^* thus depends on the values of the parameters needed to characterize these two currents. A first-order sensitivity analysis allows us to quantify the expected variation in V_m^* due to fluctuations in these parameter values. The results of this analysis are reported in Table 2. The first three columns in this table list the parameters, their values Ω, and their corresponding uncertainties $\Delta\Omega$. The derivatives listed in the fourth column are evaluated at the fixed point; they provide a mechanism for transforming parameter uncertainties into uncertainties in V_m^*. The product of the derivatives in column four with the corresponding values of $\Delta\Omega$ in column three result in the uncertainties ΔV_m^* listed in column five. Note that the location of the critical point at $V_m^* = -55.1$ mV, a slightly more depolarized membrane potential than the firing threshold at $V_f = -58$ mV, is well established within ± 2.5 mV.

It is one of our model's simplifying assumptions that an increase in dopamine results in identical modulation of the

TABLE 2. *Results of first-order sensitivity analysis*

Parameter	Ω	$\Delta\Omega$	$dV_m^*/d\Omega$	ΔV_m^*, mV
$V_h^{Kir2} - E_K$	-21 mV	2.1	0.4	0.8
V_c^{Kir2}	-11 mV	1.1	-2.3	-2.5
$\bar{g}_{Kir2}$	1.2 mS/cm^2	0.1	4.1	0.4
E_K	-90 mV	9.0	0.3	2.7
V_h^{L-Ca}	-35 mV	3.0	0.8	2.4
V_c^{L-Ca}	6.1 mV	1.0	-2.6	-2.6
$\bar{P}_{L-Ca}$	4.2 nm/s	0.7	-1.2	-0.8
$[Ca]_0$	2 μmol/cm^3	0.3	-2.5	-0.8
$[Ca]_i$	10 pmol/cm^3	1.0	0.03	0.03

maximal conductance for the Kir2 current and maximal permeability for the L-type Ca current. If we allow for the possibility that D1 dopamine receptor activation might result in unequal time courses for the modulation of the amplitude of the Kir2 and L-type Ca currents, the cancellation between these two currents will still result in a critical point. The value of V_m^* would in this case no longer arise as a solution to *Eq. 10*, but as a solution to the equation

$$\mu_{Kir2} I_{Kir2} + \mu_{L-Ca} I_{L-Ca} = 0 \quad (11)$$

where μ_{Kir2} is the conductance gain factor for the Kir2 current and $\mu_{L\text{-}Ca}$ is the permeability gain factor for the L-type Ca current. The resulting value of V_m^* will in this case depend on the ratio $(\mu_{Kir2}/\mu_{L\text{-}Ca})$; the precise location of the critical point in the $V_m - g_s$ plane of Fig. 4*B* will change accordingly. If the ratio $(\mu_{Kir2}/\mu_{L\text{-}Ca})$ is itself a function of time, the model will exhibit a dynamically generated *critical line*, a line of critical points that includes the critical point at $V_m^* = -55.1$ mV for $(\mu_{Kir2}/\mu_{L\text{-}Ca}) = 1$.

The existence of a critical point is an interesting aspect of our model. It introduces a slowdown effect that affects the dynamical response of the membrane potential to both cortical and neuromodulatory input. Although the presence of a critical point is not necessary for bistability in high dopamine conditions, its existence provides a simple explanatory mechanism for a dual response to dopamine which can either enhance or depress the response of the membrane model. We discuss this effect in detail later in this section, as we use our model to interpret the results by Kawagoe and colleagues (1998).

We conclude our discussion of dopamine-induced bistability by demonstrating the robustness of this effect. Consider the ranges of unstable values of V_m associated with the existence of unstable branches in the corresponding operational curves as shown in Fig. 4*B* for various values of μ. These unstable intervals, bounded from below by a D→U transition and from above by a U→D transition, are shown as a function of μ in Fig. 5*A*. Note the bifurcation at $\mu = 1.14$, due primarily to the Kir2 current, followed by a second bifurcation at $\mu = 1.26$, due primarily to the L-type Ca current; these two lobes coalesce at $\mu = 1.37$. The "double-S"-shaped operational curve for $\mu = 1.3$ in Fig. 4*B* is representative of this regime, in which two unstable branches are separated by a third intermediate stable branch. In spite of their intrinsic interest, the dynamical properties of the system in this regime are not especially relevant to our analysis, because they appear only for $1.26 < \mu < 1.37$ and manifest themselves only over a very narrow range $\Delta g_s \cong 0.54\ \mu S/cm^2$ of synaptic conductance. It is the wide interval of unstable values for V_m found for $\mu > 1.37$ that is especially relevant to the dopamine modulated dynamical responses of the membrane model to synaptic input.

Because the effects of D1 type dopamine receptor activation on these currents are unlikely to be strictly identical, we consider as extreme cases the possibility that only one of these two currents is affected by dopamine. As shown in Fig. 5*B*, the interplay between an enhanced L-type Ca current and the baseline Kir2 current suffices to account for most of the bifurcation diagram. The contribution of Kir2 enhancement, shown in Fig. 5*C*, is as expected restricted to hyperpolarized potentials. If both currents are simultaneously enhanced by a common factor μ, the wider unstable region in Fig. 5*A* is recovered. The analysis of Fig. 5 demonstrates that the existence of dopamine-induced bistability is a robust property of the model that does not rely on the simplifying assumption that dopamine release results in an identical enhancement of the L-type Ca and the Kir2 currents.

Dynamical responses to cortical and neuromodulatory inputs

We now investigate the dynamical evolution of the membrane potential V_m. Changes in V_m due to changes in the synaptic conductance g_s and the dopamine enhancement factor μ follow from the integration of *Eq. 1*.

We first consider the response of the membrane model to cortical inputs not associated with reward; μ remains constant at the low dopamine level ($\mu = 1$). We monitor changes in V_m in response to stepwise increases and decreases in g_s. It is under similar conditions that cortically driven transitions between the down state and the up state have been observed (Wilson and Kawaguchi 1996). The model displays such state transitions; the corresponding time constants exhibit strong dependence on the proximity of the baseline and target values of g_s to the critical point at g_s^*.

The dependence of V_m on g_s follows from *Eq. 1* for $\mu = 1$. The parameter ξ in *Eq. 7* is allowed to be a random variable so

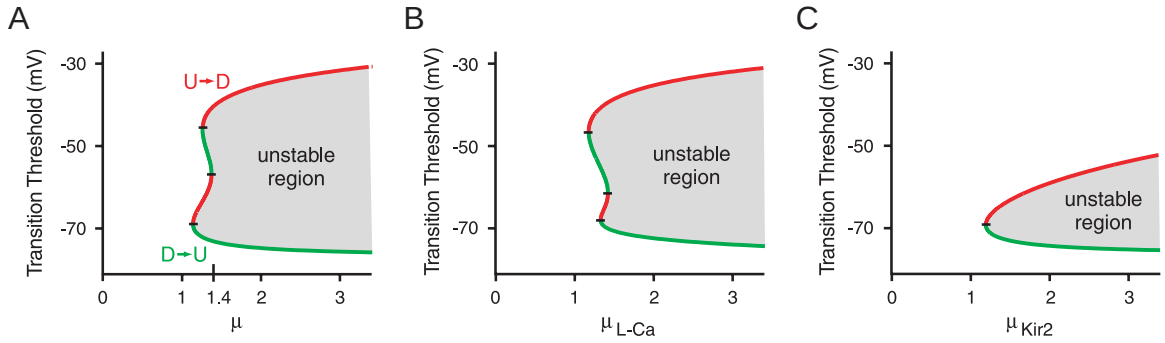

FIG. 5. Transition thresholds mark the extreme depolarized and hyperpolarized edges of the unstable regions. Green curves mark transitions from a hyperpolarized to a depolarized state (D→ U), and red curves mark transitions from a depolarized to a hyperpolarized state (U→ D). *A*: as μ increases, a bifurcation due mostly to the Kir2 current occurs at $\mu = 1.14$, followed by a 2nd bifurcation due mostly to the L-type Ca current at $\mu = 1.26$. These two coalesce at $\mu = 1.37$ into 1 larger unstable region. The interaction of baseline Kir2 conductance and enhanced L-type Ca permeability implemented through the permeability gain factor $\mu_{L\text{-}Ca}$ (*B*) or the interaction of baseline L-type Ca permeability and enhanced Kir2 conductance implemented through the conductance gain factor μ_{Kir2} (*C*) suffice to elicit membrane potential instability.

as to simulate the noisy character of synaptic input; the spike-generating model is not included. From a hyperpolarized baseline value of $V_m = -88.1$ mV for $g_s = 3\ \mu S/cm^2$ (Fig. 6*B*) and from a slightly more depolarized baseline value of $V_m = -78.7$ mV for $g_s = 10\ \mu S/cm^2$ (Fig. 6*C*), g_s is increased stepwise to values uniformly spaced between 10 and 22.5 $\mu S/cm^2$. These instantaneous increases in g_s are followed by slower increases in the membrane potential V_m as it moves toward its equilibrium value. After 400 ms, the value of g_s is instantaneously returned to its baseline value, and V_m decays back toward its original value. We show in Fig. 6*A* two of the corresponding trajectories in the $V_m - g_s$ plane. One trajectory (squares) describes the evolution of the system from a baseline value of $g_s = 3\ \mu S/cm^2$ to an increased value of $g_s = 12.5\ \mu S/cm^2$ and back; a second trajectory (diamonds) describes the evolution of the system from a baseline value of $g_s = 10\ \mu S/cm^2$ to an increased value of $g_s = 17.5\ \mu S/cm^2$ and back.

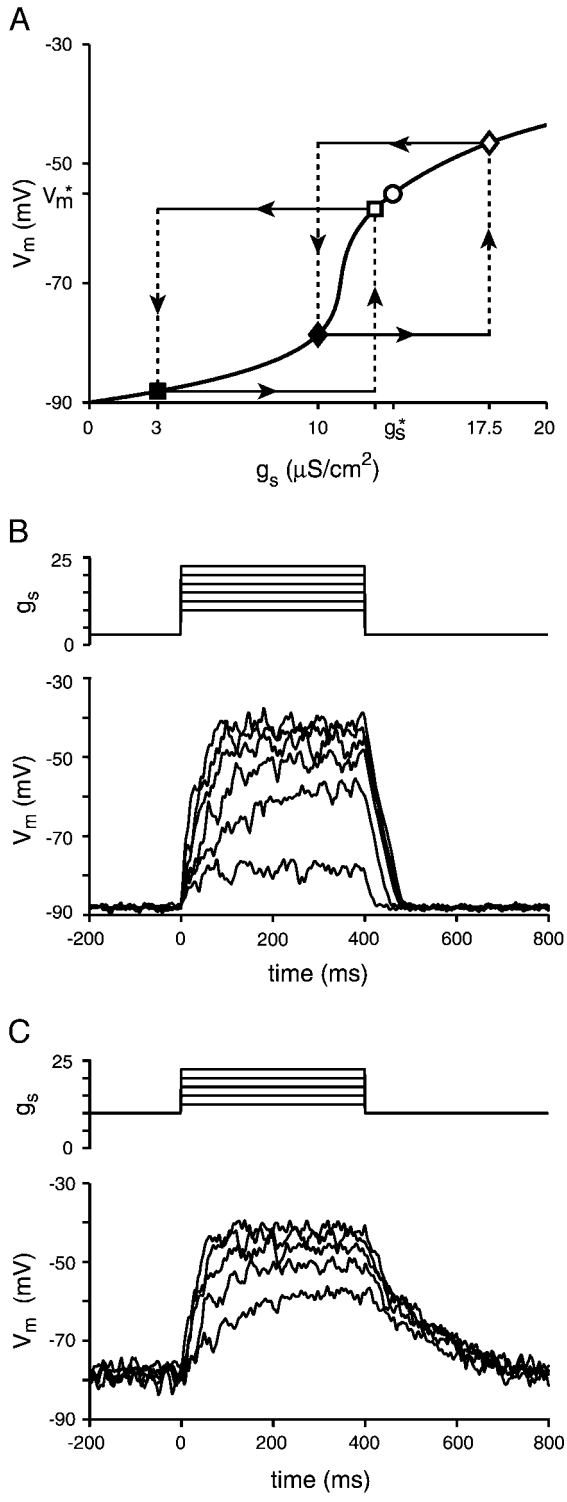

Changes in synaptic conductances and the resulting membrane potential traces are shown in Fig. 6, *B* and *C*. Rapid fluctuations in V_m are due to the inclusion of synaptic noise. Some of these traces exhibit a noticeable slowdown during depolarization. This *critical slowing down* is a generic consequence of the existence of a critical point. The effect is particularly noticeable whenever trajectories in the $V_m - g_s$ plane, such as those shown in Fig. 6*A*, pass near the critical point. Depolarizing trajectories triggered by increases in the synaptic conductance up to a value of $g_s = 12.5$ or 15 $\mu S/cm^2$ come close to the critical point at $g_s^* = 13.28\ \mu S/cm^2$, and the dynamical convergence of V_m to its new equilibrium value is slow (see the corresponding traces in Fig. 6, *B* and *C*). Depolarizing trajectories triggered by increases in g_s to values further removed from g_s^* do not exhibit this slowdown effect. All hyperpolarizing trajectories returning to a baseline of $g_s = 10\ \mu S/cm^2$ pass much closer to the critical point than those returning to a baseline of $g_s = 3\ \mu S/cm^2$ (see Fig. 6*A*). It is this proximity to the critical point that explains the slowdown in the hyperpolarizing V_m traces in Fig. 6*C* not observed in the hyperpolarizing V_m traces in Fig. 6*B*.

We now consider the dynamical response of the membrane model to changes in dopamine level; the cortical input g_s is kept constant while the dopamine-controlled neuromodulatory factor μ varies with time. These conditions mimic those of experiments that monitor the modulation of tonic striatal activity due to the application of dopaminergic agents or due to the electrical stimulation of dopamine fibers (Gonon 1997; Kiyatkin and Rebec 1996; Williams and Millar 1990). This set of numerical experiments displays dramatic dynamical slowdown for g_s close to g_s^* (Fig. 7). The results also reveal a novel effect: increased dopamine levels can result in either depolarization or hyperpolarization depending on whether g_s does or does not exceed g_s^*.

FIG. 6. Dynamic responses of V_m to step changes of g_s at $\mu = 1$. In these experiments, g_s is increased from a baseline level to a step level of 10, 12.5, 15, 17.5, 20, and 22.5 $\mu S/cm^2$ for 400 ms and then is returned to baseline. *A*: sample trajectories corresponding to 1 experiment in *B* (squares) and 1 in *C* (diamonds). The open circle identifies the critical point. *B*: in these experiments, g_s is increased in steps from a baseline of 3 $\mu S/cm^2$. For the 2nd trajectory from the bottom, g_s is increased to 12.5 $\mu S/cm^2$. The instantaneous increase in g_s at $t = 0$ corresponds to the horizontal line that originates at the filled square in *A*; V_m reacts to this change by depolarizing along the vertical dashed line toward the open square. The close proximity to the critical point slows down the depolarization process. A subsequent step decrease to the baseline level leads to hyperpolarization along the dashed vertical line toward the filled square. This process is fast, as are the other hyperpolarizing processes shown in *B*, because they occur away from the critical point. The characteristic rate for the depolarizing processes depends on the proximity of the corresponding trajectories to the critical point. *C*: in these experiments, g_s is increased in steps from a baseline of 10 $\mu S/cm^2$. For the 3rd trajectory from the bottom, g_s is increased to 17.5 $\mu S/cm^2$. The corresponding trajectory originates at the filled diamond in *A* and depolarizes to the open diamond. The characteristic rate for the depolarizing processes depends on the proximity of the corresponding trajectories to the critical point. The hyperpolarizing processes are slow because all vertical trajectories terminating at the filled diamond are close to the critical point.

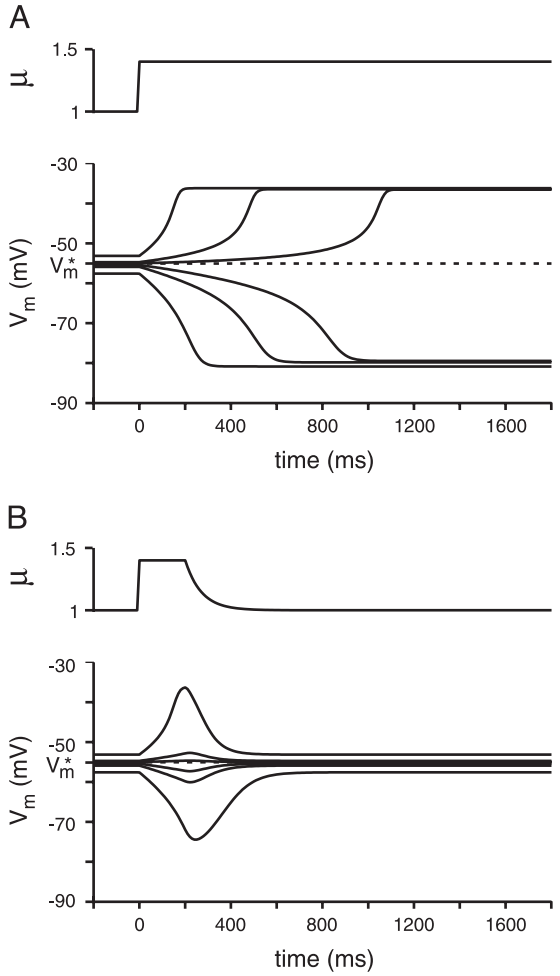

FIG. 7. Dynamic responses of V_m to changes in μ at fixed g_s; the values of g_s are close to the critical g_s^*. *A*: in these experiments, μ is increased in a step from $\mu = 1$ to 1.4. The cell membrane depolarizes for $g_s > g_s^*$ and hyperpolarizes for $g_s < g_s^*$. These processes become increasingly slow as the value of g_s approaches g_s^*. *B*: in these experiments, μ is increased in a step from $\mu = 1$ to 1.4 for 200 ms and allowed to decay to its baseline level with a time constant of 70 ms. The transient response is depolarizing (hyperpolarizing) for $g_s > g_s^*$ ($g_s < g_s^*$). Transient responses slow down and barely have time to develop as the value of g_s approaches g_s^*.

In this set of numerical experiments, the synaptic conductance g_s is held constant and no synaptic noise is included ($\xi = 1$ in *Eq. 7*). Changes in the membrane potential V_m are triggered by changes in μ. We consider two different scenarios. In the first case (Fig. 7*A*), μ increases abruptly from $\mu = 1$ to $\mu = 1.4$ at $t = 0$, and it then remains constant at this high value. In the second case (Fig. 7*B*), μ again increases abruptly from $\mu = 1$ to $\mu = 1.4$ at $t = 0$, remains fixed at this high value for 200 ms, and then relaxes exponentially back to $\mu = 1$ with a time constant of $\tau = 70$ ms.

The membrane potential traces in Fig. 7*A* show that the response of the system to an increase in μ from $\mu = 1$ to $\mu = 1.4$ can be either a depolarization or a hyperpolarization, depending on the state of the system when the change in μ takes place. If the value of g_s exceeds $g_s^* = 13.28$ μS/cm^2, the equilibrium value of V_m at $\mu = 1$ exceeds V_m^*; in this case, the membrane depolarizes when μ is increased. If the value of g_s is smaller than g_s^*, the equilibrium value of V_m at $\mu = 1$ is smaller than V_m^*; in this case, the membrane hyperpolarizes when μ is increased. Note also that the time course of membrane potential dynamics is strongly affected by the critical point. The closer the equilibrium value of V_m at $\mu = 1$ is to V_m^*, the longer it takes for the membrane potential to reach its new equilibrium value corresponding to $\mu = 1.4$.

The membrane potential traces in Fig. 7*B* illustrate the interplay between the dynamics of μ and the slowdown in the dynamics of V_m in the vicinity of the critical point. If the equilibrium value of V_m at $\mu = 1$ is close to V_m^*, the response to an increase to $\mu = 1.4$ is so slow that the membrane potential has barely changed by the time μ begins to relax back toward $\mu = 1$. Significant transient depolarizing or hyperpolarizing effects can only be observed when the membrane potential at $t = 0$ is further removed from V_m^*.

The dynamical slowdown effects illustrated in Figs. 6 and 7 are a generic consequence of the existence of a critical point. As shown in Fig. 3*C*, the total current that determines the rate dV_m/dt at which V_m changes is close to zero for a range of values of V_m around V_m^* if g_s is close to g_s^*. It is the approximate cancellation of the Kir2 and L-type Ca currents in the vicinity of the critical point that results in low values for dV_m/dt and the ensuing slowdown in the dynamical response of the membrane model.

Dopamine-mediated modulation of cortically driven responses

We now discuss the response of the membrane model to combined cortical and dopamine inputs analogous to those that occur when reward is anticipated by an awake animal (Fig. 1). In the preceding section, we described dynamical responses first to cortical inputs in the absence of dopamine neuromodulation and then to dopamine neuromodulation when cortical input was held fixed at different values. In this section, we provide a generic description of the response to sensory cues that trigger both phasic cortical input and dopamine release. The analysis of this scenario demonstrates that the expectation of reward can result in either enhancement or suppression of membrane model responses. In the following section, we present a numerical experiment that incorporates the various aspects of signal integration summarized in Fig. 1, including quantitative timing information, in a simulation of single-unit responses for comparison to those reported by Kawagoe and colleagues.

Consider a scenario in which a tonically active context signal maintains V_m below the firing threshold V_f. A target signal of finite duration and sufficient amplitude to drive V_m above V_f is added to the context signal. The response of the model to this combined synaptic input is critically dependent on the expectation of reward.

Two cases are of particular significance: whether the combined synaptic input exceeds (Fig. 8*A*) the value of $g_s = 14.17$ μS/cm^2 for the D→U transition or whether it remains below (Fig. 8*B*) the critical value $g_s^* = 13.28$ μS/cm^2. If the phasic input is not associated with a reward, the dopamine level does not increase and $\mu = 1$ (Fig. 8, *left*); the operational curve that represents equilibrium values of the membrane potential V_m as a function of the total synaptic input g_s remains unchanged (dotted curve). In unrewarded trials, the only difference between a larger and a smaller target input is that the former results in a more depolarized membrane potential and thus in a

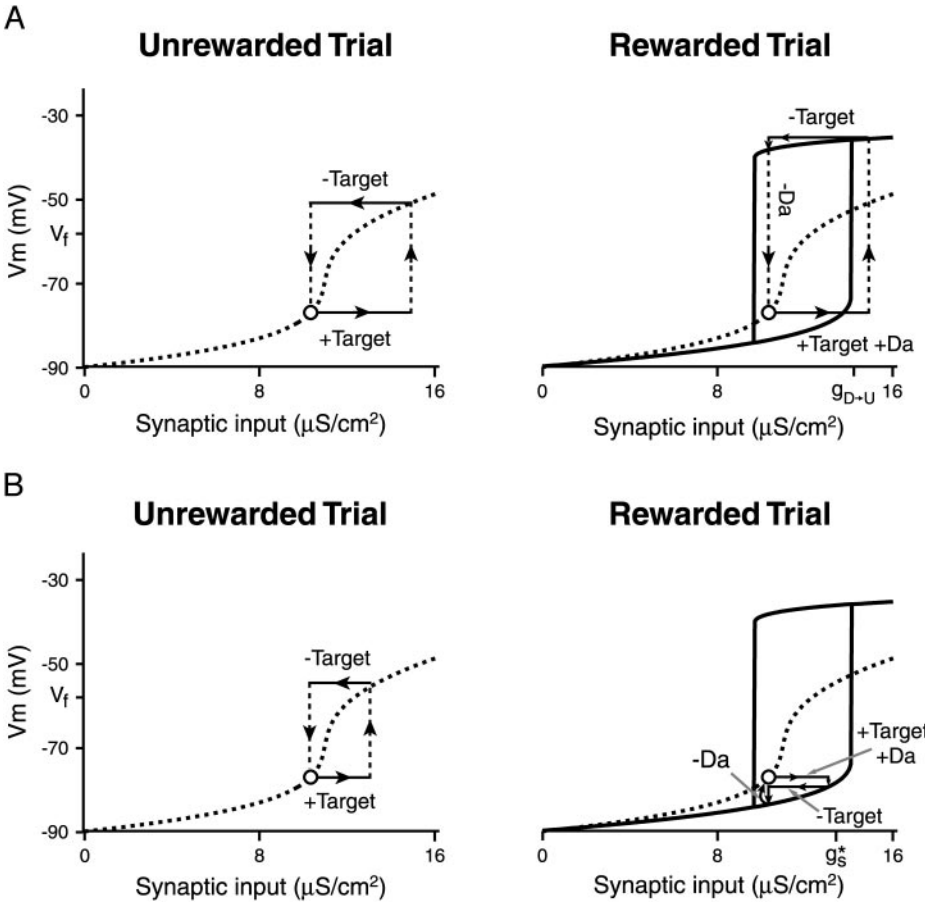

FIG. 8. Responses to target input in unrewarded (*left*) and rewarded (*right*) trials. A tonic context signal depolarizes the unit to a level below the firing threshold at $V_f = -58$ mV. *A*: a phasic target signal is added to the context signal; the total input is $g_t + g_c > g_{D\to U}$. If the target is not associated with a reward, its onset results in depolarization toward the $\mu = 1$ operational curve (*left*); the equilibrium value of V_m exceeds V_f. The response lasts for the duration of the target presentation. If the target is a conditioned stimulus, its onset elicits dopamine release. The operational curve changes from a sigmoidal ($\mu = 1$) to a bistable ($\mu = 1.4$) form (*right*). Because $g_s > g_{D\to U}$, the unit depolarizes toward the upper branch of the bistable curve. The resulting enhanced response is sustained until μ relaxes back to its baseline level if $g_c > g_{D\to U}$. *B*: a phasic target signal is added to the context signal; the total input is $g_t + g_c < g_s^*$. If the target is not associated with a reward (*left*), its onset results in activity very similar in nature but smaller in intensity than the one triggered by the larger unrewarded target in *A*; the level of activity in unrewarded trials encodes for the amplitude of the phasic signal. If the target is a conditioned stimulus, the operational curve becomes bistable (*right*). Because $g_s < g_s^*$, the unit hyperpolarizes toward the lower branch of the bistable curve; activity is suppressed.

higher firing rate. This firing activity, which quickly decays when the target signal disappears, encodes for the strength of the target stimulus.

Rewarded trials (Fig. 8, *right*) elicit different responses. In these trials, target onset serves as the conditioned stimulus that triggers dopamine release in the striatum. In elevated dopamine conditions, the operational curve changes from the $\mu = 1$ (dotted) curve to the bistable $\mu = 1.4$ (solid) curve. The consequences of this switch to a bistable operational curve depend on the strength of the target input.

If the combined synaptic input exceeds the value for the D→U transition in a rewarded trial (Fig. 8*A*, *right*), the resulting depolarization in membrane potential does not end at the intersection with the dotted curve for $\mu = 1$ but continues until V_m reaches the upper branch of the bistable operational curve. This additional depolarization results in a noticeably higher firing rate than the one elicited by the same value of g_t in the unrewarded trial (Fig. 8*A*, *left*). Thus whenever the condition $g_c + g_t \geq g_{D\to U}$ is met, dopamine will enhance the response of the model to the reward-predicting target. When the target signal is removed, the membrane hyperpolarizes slightly as V_m moves down toward the upper branch of the bistable operational curve. If the context signal provides an input that exceeds that of the U→D transition, V_m remains in the up state until μ decreases toward its baseline level. In a rewarded trial, the response is not only larger in amplitude, but it can also be longer in duration.

If the combined synaptic input is not sufficient to exceed the critical value of $g_s^* = 13.28$ μS/cm^2, the response will always be a hyperpolarizing one (Fig. 7); V_m will decrease toward the lower branch of the bistable operating curve (Fig. 8*B*, *right*) and remain in this hyperpolarized state until μ decreases toward its baseline level. For this type of rewarded trial, dopamine suppresses the response of the model.

The analysis presented in the preceding text provides an explanatory mechanism for the observation of either enhanced or suppressed spiny neuron activity in the presence of dopamine. It is the strength of the total synaptic input that selects between these two effects; the generic features of this differentiation are summarized in Fig. 9. Enhancement occurs when the total synaptic input exceeds the threshold for the D→U transition, while suppression occurs when the total synaptic input is lower than the one corresponding to the critical point. The separatrix, which marks the boundary between enhancement and suppression, will always lie in the narrow band (Fig. 9, shaded area) limited by $g_c + g_t = g_{D\to U}$ and $g_c + g_t = g_s^*$. The precise location of the separatrix will depend on the details of the temporal evolution of μ as it rises and returns to baseline. An examination of the family of operational curves shown in Fig. 4*B* reveals that if $\mu(t)$ increases slowly, the separatrix will lie close to the $g_c + g_t = g_s^*$ line, whereas if $\mu(t)$ increases rapidly, the separatrix will lie close to the $g_c + g_t = g_{D\to U}$ line. But whatever the shape of $\mu(t)$ might be, there will be a range of values of g_s for which activity is suppressed, and a different range of values of g_s for which activity is enhanced. The strength of this conclusion follows from the generic nature of our argument, which does not rely on assumptions about the specific time course $\mu(t)$ of dopamine neuromodulatory effects.

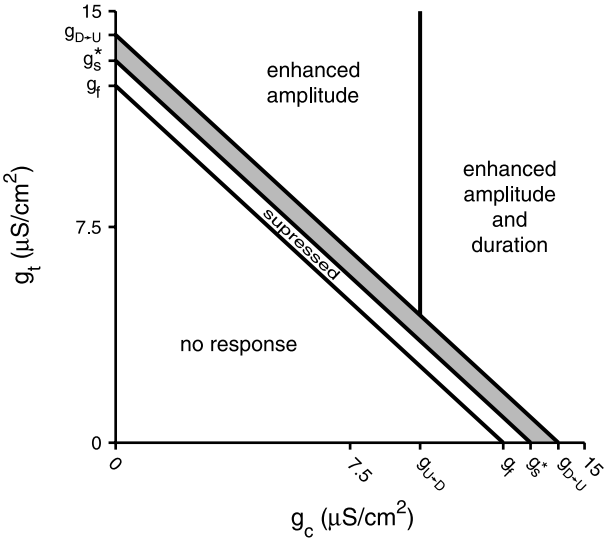

FIG. 9. The modification of unit response as dopamine is elevated (μ = 1.4) from baseline levels (μ = 1) depends on context and target signals. There is no response for total input ($g_t + g_c$) smaller than the input g_f needed to reach the firing threshold at V_f. The activity that would be elicited for total input larger than g_f at μ = 1 is suppressed for μ = 1.4 if the total input does not exceed g_s^*. If the total input exceeds $g_{D\to U}$, responses are enhanced for μ = 1.4. If g_c exceeds $g_{U\to D}$, the enhanced response is maintained longer. The effect of dopamine on the unit's response for total input larger than g_s^* but smaller than $g_{D\to U}$ (shaded area) depends on the details of the dynamical evolution of both g_s and μ.

Modulation of single-unit activity by expectation of reward

We now investigate the responses of our model in a scenario that simulates the memory-guided saccade task described by Kawagoe and colleagues (1998). In this task (see Fig. 1), a visual target is presented for 100 ms; this type of brief visual stimulus elicits cortical activity that follows the onset of the stimulus after a 100 ms delay and lasts for ~400 ms (Colby et al. 1996). This stimulus may or may not be associated with the expectation of reward. If it is, it triggers a brief burst of SNpc dopamine neuron activity that also follows the onset of the stimulus after a 100 ms delay (Schultz et al. 1993).

The discharge of SNpc neurons produces dopamine transients in the striatum similar to those elicited by electrical stimulation of the medial forebrain bundle, which can lead to bouts of spiny neuron activity that begin after 200 ms and decay back to baseline within 1,000 ms (Gonon 1997). In our model, this dopamine-induced enhancement of spiny neuron activity is attributed to an increase in Kir2 and L-type Ca currents mediated through D1 receptor activation (Pacheco-Cano et al. 1996; Surmeier et al. 1995) and the subsequent interactions of second messengers. Both the lag due to second-messenger processes and the delays associated with the dynamical response of the membrane potential contribute to the 200 ms latency observed (Gonon 1997) in spiny neuron responses to dopamine. Such short-term modulatory effects are incorporated in our model through the dopamine-controlled neuromodulatory factor μ, whose time course is chosen based on the experimental observations summarized in the preceding text.

The numerical experiments shown in Fig. 10 display the response of the model neuron to cortical inputs in both unrewarded (*left*) and rewarded (*right*) trials; we choose a form of $\mu(t)$ appropriate for each of these cases. A constant value of $\mu(t)$ = 1 corresponds to low dopamine conditions characteristic of unrewarded trials (Fig. 10, *left*). For rewarded trials (Fig. 10, *right*), we keep $\mu(t)$ at its baseline μ = 1 value for an additional 80 ms after the onset of the discharge of dopamine neurons; this delay is followed by an exponential rise toward μ = 1.4 with a time constant of 70 ms. An exponential decay toward μ = 1 with a time constant of 100 ms begins 600 ms after the onset of the exponential rise.

The model neuron receives two types of excitatory cortical input. In addition to a tonic background input that represents context-related cortical activity, there is a phasic cortical input that represents cortical responses to a 100 ms-long visual stimulus; this transient input lags by 100 ms and lasts for 400 ms. We choose g_c = 10.5 μS/cm^2, which exceeds $g_{U\to D}$ = 9.79 μS/cm^2, and consider two possible strengths for the phasic input: a high value of g_t = 3.8 μS/cm^2 (Fig. 10*A*), for which $g_s = g_c + g_t$ = 14.3 μS/cm^2 exceeds $g_{D\to U}$ = 14.17 μS/cm^2 and a low value of g_t = 2.4 μS/cm^2 (Fig. 10*B*), for which $g_s = g_c + g_t$ = 12.9 μS/cm^2 is below g_s^* = 13.28 μS/cm^2. For each one of these four cases, we show in Fig. 10 representative membrane potential traces, spike rasters for 30 independent realizations, and the resulting poststimulus time histogram.

For g_t = 3.8 μS/cm^2 (Fig. 10*A*), the membrane potential crosses the firing threshold ~100 ms after the onset of phasic cortical input. In unrewarded trials (*left*), firing is sustained by the phasic cortical input and stops after its offset. In rewarded trials (*right*), the membrane potential again crosses the firing threshold ~100 ms after the onset of phasic cortical input, and firing begins in a manner quite similar to that observed in the corresponding unrewarded trial. But 200 ms after the onset of dopamine discharge, the membrane potential reacts to elevated dopamine, resulting in a prominent enhancement of spiny neuron activity. This enhancement persists for ~400 ms beyond the offset of the phasic cortical input; this extended duration is due to the hysteretic effect of bistability (see Fig. 8*A*).

For g_t = 2.4 μS/cm^2 (Fig. 10*B*), the membrane potential crosses the firing threshold ~130 ms after the onset of phasic cortical input. In unrewarded trials (*left*), the spiny neuron displays a small amount of activity, less than that observed in the unrewarded trial for g_t = 3.8 μS/cm^2. This activity is sustained by the phasic cortical input, and it ceases following its offset. For unrewarded trials, the firing rate of the model spiny neuron encodes for the strength of g_t. In rewarded trials (*right*), the low-level activity that begins to build up ~130 ms after the onset of the phasic cortical input is nearly completely suppressed by the effect of elevated dopamine.

The results in Fig. 10 are to be compared with the experimental data from Kawagoe and colleagues (1998; see Figs. 2 and 3). Except for the spatial tuning, which is not included in our present model, the responses of the model spiny neuron reproduce most of the trends displayed by the experimental single-unit data.

DISCUSSION

The model presented in this paper was designed to focus on the short-term effects of dopamine neuromodulation in the soma of striatal medium spiny neurons through D1 receptor activation. We used this model to test the hypothesis that the reward-dependent activity of dopamine neurons, and the subsequent effects of dopamine release on Kir2 and L-type Ca

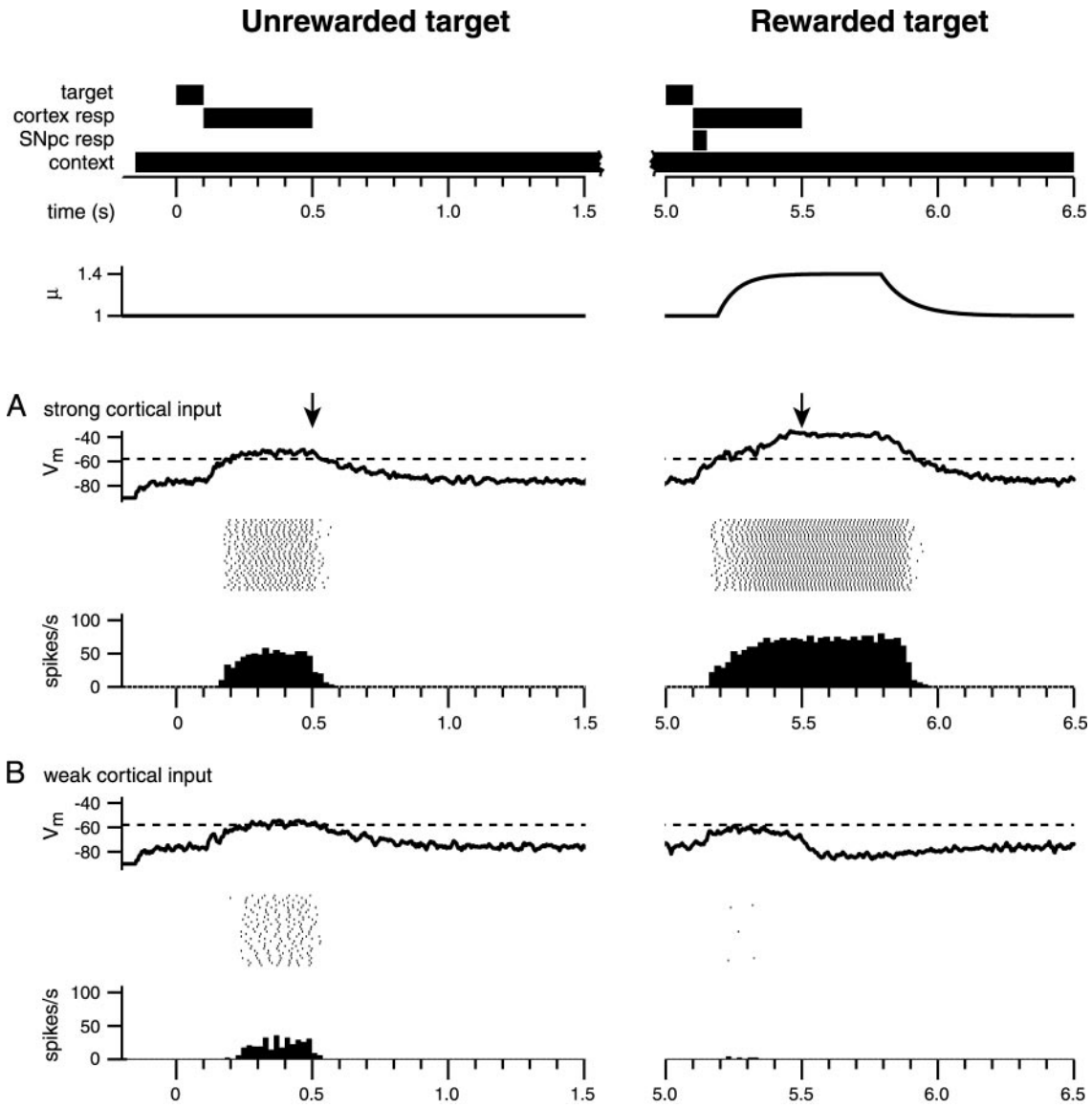

FIG. 10. Simulated responses to target input in unrewarded (*left*) and rewarded (*right*) trials. A constant background input represents context-related cortical activity. The presentation of a visual target for 100 ms elicits a phasic cortical response that lags by 100 ms and lasts for 400 ms. The ↓ in *A* indicate the offset of phasic cortical input. Rewarded targets also trigger the response of substantia nigra pars compacta dopamine neurons with a lag of 100 ms, which results in a transient increase of $\mu(t)$ above its baseline value of $\mu = 1$. We choose $g_c = 10.5\ \mu S/cm^2$, which exceeds $g_{U\to D} = 9.79\ \mu S/cm^2$, and consider two possible strengths for the phasic input: $g_t = 3.8\ \mu S/cm^2$, for which $g_s = g_c + g_t = 14.3\ \mu S/cm^2$ exceeds $g_{D\to U} = 14.17\ \mu S/cm^2$ (*A*) and $g_t = 2.4\ \mu S/cm^2$, for which $g_s = g_c + g_t = 12.9\ \mu S/cm^2$ is below $g_s^* = 13.28\ \mu S/cm^2$ (*B*). Representative membrane potential traces, spike rasters for 30 independent realizations, and the resulting poststimulus time histogram are shown for each one of these four cases.

currents via D1 receptors, can account for both the enhancement and the suppression of single-unit responses recorded in the striatum. The model is an abstraction of the complex mechanisms that control spiny neuron discharge in the intact animal. Care was taken to include an experimentally based representation of specific neuromodulatory effects of D1 receptor activation together with a biophysically grounded description of the steady-state behavior of relevant ionic currents in the intermediate time scale of 100–1,000 ms. The resultant minimal model predicts that the effects of dopamine on D1 receptors result in a qualitative change in the properties of medium spiny neurons: dopamine induces the emergence of bistability in the operational curves of the model. We further demonstrate that the anticipated degree of bistability can account for both enhancement and depression of spiny neuron discharge in awake animals that are engaged in selectively rewarded tasks. Our analysis shows that this complex reward dependence is a generic consequence of the bistability that arises in high dopamine conditions for a wide range of model parameters. The introduction of a spiking mechanism and of biologically appropriate timing information for cortical and dopamine inputs allows the model to reproduce the qualitative features of rasters in the Kawagoe data.

Ionic currents and membrane model properties

Our model is based on ion current data from acutely isolated cells, in which only the soma and proximal dendrities are

preserved (Bargas et al. 1994). Although both L-type calcium and Kir2 channels are prominent in dendritic regions (Hell et al. 1993; Nisenbaum and Wilson 1995), we cannot exclude the possibility that there are dendritic conductances of importance to state transitions that have not been included. In spite of this potential limitation, the model does mimic characteristic features of spiny neuron electrophysiology.

In the low dopamine condition, the model is consistent with the characterization of medium spiny neurons as being bimodal as opposed to truly bistable (Wilson and Kawaguchi 1996). The interaction of the Kir2 and Ksi potassium currents results in a steep slope in the membrane potential as a function of synaptic conductance for potentials intermediate to those characteristic of the up state and down state (dotted curve in Fig. 4*A*); the change in membrane potential between these two values takes place over a fairly narrow range of synaptic conductances (bimodal behavior). The time course of the model's transitions between down and up states (Fig. 6) shows a critical slowing down that appears to be in agreement with the experimental literature. Wilson (1993; see Fig. 5) illustrates a down to up state transition that is slower than the up to down state transition; this is the behavior exhibited by the second and third (from the bottom) membrane potential traces in Fig. 6*B*. In contrast, Wilson and Kawaguchi (1996; see Fig. 4) show down to up state transitions that are faster than up to down state transitions; this is the behavior exhibited by the first, second, and third (from the top) membrane potential traces in Fig. 6*C*. Our model predicts that these differences result from different levels of tonic (context) input from cortex (Fig. 1) in the two sets of experiments. A potential test of the model would be to repeat the Wilson experiments in a preparation in which the tonic (background) synaptic input from the cortex is systematically varied, perhaps through the application of pharmacological agents to the cortex.

In the high dopamine condition, a modest increase of Kir2 and L-type Ca currents causes the model to undergo a bifurcation and become bistable (solid curve in Fig. 4*A*). While the membrane potential characteristic of the down state is only moderately affected by dopamine, the model predicts a substantial additional depolarization of the up state in the presence of elevated dopamine in contrast to the low dopamine condition in which the up state is typically characterized. The membrane potential of the up state in the high dopamine condition is above the firing threshold and is therefore not observable as a steady state in spiny neurons; the fast dynamic properties of the currents involved in the generation of action potentials prevent the membrane potential from converging to this depolarized fixed point. A possible way to test for this additional depolarization would be to repeat the Gonon (1997) experiment using patch-clamp recording electrodes filled with QX314 to block action potentials.

Several currents that are not included in the model contribute to the generation of action potentials and repetitive firing. These currents could modulate the model's responses. For example, the depolarization of the up state in high dopamine conditions could be diminished by K^+ currents not included in the model, such as other K^+ currents or Ca^{2+}-activated K^+ currents involved in afterhyperpolarization potentials (AHPs). Other currents that are active during the up state and during spiking include Na^+ currents and N/P-type Ca^{2+} currents. The inclusion of these inward currents could in principle enhance the mechanisms responsible for bistability. However, these currents are modulated by D1 receptor activation: transient Na^+ and N/P-Q type Ca^{2+} currents are reduced (Surmeier and Kitai 1993; Surmeier et al. 1995). Because the suppression of transient Na^+ currents is mediated by enhanced entry of Na^+ channels into a slow inactivated state (D. Carr, M. Day, A. R. Cantrell, T. Scheuer, W. A. Catterall, and D. J. Surmeier, unpublished data), the consequences of this modulation should be to reduce discharge rate late in an up-state episode. As such, it will not qualitatively change our conclusions. As for N/P-Q Ca^{2+} currents, these are activated by spiking and control Ca^{2+}-dependent K^+ channels regulating repetitive firing (Vilchis et al. 2000). Hence, D1 receptor-mediated suppression of these Ca^{2+} currents should enhance the up-state depolarization and repetitive discharge, in agreement with model predictions. Nevertheless, a model including more biophysical detail would be necessary to investigate the *quantitative* effects of elevated dopamine on such short time scale phenomena. This is not our goal; the *qualitative* features of reward-dependent activity that we wish to describe follow from the simple assumption that more depolarized states result in higher firing rates. Within this approach, the specific values for the parameters V_h and V_c that control the firing rate in our model are not too significant; they control only the relative amplitude of the responses in Fig. 10 but do not affect the generic features of the reward dependence resulting from dopamine-induced bistability.

Although there are many currents that control the membrane potential of spiny neurons, of which several are modulated by dopamine, our model includes only two dopamine-modulated currents, Kir2 and L-type Ca, and the unmodulated Ksi current that stabilizes the up state. This minimal model is designed to investigate whether the D1 mediated modulation of these two currents suffices to account for the qualitative features of dopamine modulation of spiny neuron responses at intermediate time scales. Our model predicts the emergence of bistability in the membrane potential of spiny neurons; this is a novel phenomenon for which there is only limited experimental evidence. Sustained depolarization after brief current injection in the presence of D1 agonists has been observed in vitro (Hernandez-Lopez et al. 1997); such sustained depolarizations, to be distinguished from transitions to the up state due to a barrage of synaptic inputs in low dopamine conditions, are a hallmark of bistable responsiveness. Recent experimental results (Hernandez et al. 2002) give further evidence for dopaminergic modulation of bistable behavior in medium spiny neurons.

Comparison of model and single-unit activity

The response properties of the model neuron are qualitatively similar to those of neostriatal spiny neurons reported by Kawagoe and colleagues (1998). They observed that spiny neurons show directional tuning to spatially separated targets in a saccade task and that these responses are strongly modulated by the expectation of receiving or not receiving a reward as reinforcement. Two types of response modulation were reported. Most units show a more intense response of longer duration to a given target in blocks of trials in which saccades to that target elicit a liquid reward (primary reinforcement) as opposed to auditory feedback (secondary reinforcement). A

few units show instead suppressed activity to the presentation of targets in the rewarded case. The response properties of the model are consistent with the basic features of these experimental observations. The model identifies the strength of the total excitatory cortical input as the experimental parameter that selects between these two types of modulation in rewarded trials, and it predicts the existence of a separatrix that lies in a narrow range of total input between the critical conductance g_s^* and the conductance $g_{D\rightarrow U}$ at the down to up state transition. If the total synaptic input exceeds the separatrix in rewarded trials, the membrane depolarizes toward the upper branch of the hysteresis curve and activity is enhanced. If the total synaptic input falls below the separatrix, the membrane hyperpolarizes toward the lower branch and activity is suppressed. An ensuing feature is that enhanced responses can have a range of amplitudes, depending on the properties of the spike generating mechanism, but attenuated responses lead to a nearly complete suppression of activity for most values of the cortical input below the separatrix. This is in agreement with the Kawagoe (1998) data; they report facilitated responses of many frequencies but attenuations almost always close to total suppression.

The activation of D1 receptors can lead to moderate as opposed to total suppression of tonic spiny neuron activity (Hu and Wang 1988; Rebec 1998). The model provides two mechanisms that could account for this observation. The first one is a dynamical effect due to the slow membrane responses associated with the existence of a critical point. Consider a low-dopamine equilibrium state at a value of V_m slightly more hyperpolarized than V_m^*; a transient increase in dopamine results in a moderate suppression of activity due to a small amplitude dip in the membrane potential (see Fig. 7*B*). The slow nature of the dopamine-triggered hyperpolarization prevents the membrane potential from reaching the highly hyperpolarized equilibrium state associated with total suppression. The second mechanism is a static effect based on variations in the strength of dopaminergic modulation, represented in our model by the maximal value μ^{max} of the neuromodulatory factor μ. Consider again a low dopamine equilibrium state at a value of V_m slightly more hyperpolarized than V_m^*. A moderate increase in dopamine, characterized by values of μ^{max} smaller than ~1.3, results in a hyperpolarized shift of the corresponding stable fixed point, as seen in Fig. 4*B* for $\mu^{max} = 1.1$, 1.2, and 1.3. Units that exhibit levels of V_m greater than threshold but below V_m^* at $\mu = 1$ will remain active but at lower rate in such moderately elevated dopamine conditions.

In contrast to the effect discussed in the preceding text, an increase in the value of μ^{max} would result in a wider bistable region with an upper bound at a higher value of the conductance threshold $g_{D\rightarrow U}$ for the down to up state transition; this widens the shaded area in Fig. 9. A given excitatory input could then result in a value of g that exceeds the value of $g_{D\rightarrow U}$ for a smaller value of μ^{max} but is below the value of $g_{D\rightarrow U}$ for a larger value of μ^{max}. Such an input would correspond to a point above the shaded area in Fig. 9 in the former case but within the shaded area in the latter. If this input triggers dopamine release, the response will be enhanced in the former case but could be suppressed in the latter. This property of the model is consistent with data showing that whereas low concentrations of exogenously applied dopamine or low stimulation of dopamine neurons can enhance spiny neuron activity, high concentrations or large stimulation can suppress activity in the same neuron (Williams and Millar 1990). A variability in the value of μ^{max} associated with different neurons can represent different levels of dopaminergic modulation in a population; spiny neurons with a large value of μ^{max} can account for the observation that some units reported by Kawagoe et al. (1998) exhibit high activity in unrewarded trials yet are suppressed in rewarded trials.

The model also suggests a temporal correlation that is consistent with the data. Dopamine-induced bistability in conjunction with a sufficiently strong context input maintains the model neuron in the depolarized up state after the target is extinguished, which extends the duration of the enhanced response. The duration of the response is then dependent on the time course of the neuromodulatory factor μ. A similar time correlation may be present in spiny neurons. The duration of high-frequency activity apparent in the enhanced single-unit response in rewarded trials (Kawagoe et al. 1998) is at least as long as the time course of elevated dopamine in the striatum elicited by burst activity of dopamine neurons (Dugast et al. 1994; Gonon 1997).

In contrast to the hypothesis that D1 receptor activation can mediate both enhancement and suppression of striatal activity, Kawagoe and colleagues (1998) suggest that the observation of facilitated and suppressed responses in rewarded trials is the result of different effects of D1 and D2 receptor activation on the activity of spiny neurons. Their hypothesis is that the response of neurons that possess mostly D2 receptors will be suppressed in rewarded trials, whereas the response of those with mostly D1 receptors will be enhanced. This conjecture is consistent with recent evidence that D2 receptor activation reduces Na^+ and L-type Ca currents, which reduces spiny neuron excitability (Hernandez-Lopez et al. 2000; Kiyatkin and Rebec 1999; Maurice et al. 2001), and is also consistent with the potentiating effect of D1 receptor activation, but it ignores evidence indicating that D1 activation can also exert a suppressive effect (Hernandez-Lopez et al. 1997; Hu and Wang 1988). Most spiny neurons express either mostly D1 or mostly D2 type receptors (Gerfen et al. 1990; Surmeier et al. 1996). The model presented here applies to spiny neurons that express mostly D1 receptors, and it can explain both enhanced and suppressed spiny neuron activity in response to conditioned stimuli. However, our results do not preclude a suppression of activity mediated by D2 receptor activation.

In our model, the properties of membrane response follow from the dynamical interplay between the strength of excitatory input and the degree of dopamine modulation; while dopamine modifies the operational curve that defines the response properties, it is the total cortical input that selects between enhancement and suppression. The hypothesis that the amount of excitatory input selects the modulated response type has been offered as an explanation for the in vivo observation that dopamine affects the response of striatal units in different amounts (Kiyatkin and Rebec 1996) or in qualitatively different manner (Pierce and Rebec 1995). These ideas could be tested by correlating the level of excitatory input with the observation of enhanced or suppressed activity in elevated dopamine conditions. A direct measure of the excitatory input could be obtained through voltage clamp at hyperpolarized potentials. An indirect measure could be obtained by manipulating the level of cortical activity through the application of

pharmaceuticals. This approach could allow for the observation of enhanced responses becoming suppressed as the level of cortical activity is reduced. The functional consequences of excitatory input selected modulation will be discussed in a later section.

Other dopaminergic effects in the striatum

There is a large corps of data demonstrating that dopamine can influence the activity of neurons in many ways. The model presented here is intended to represent the actions of dopamine in a specific context: the modulatory effects of phasic D1 receptor activation on the short-term response properties of medium spiny neurons. This model can be expanded to include other actions of dopamine in the striatum, such as the short- and long-term actions of dopamine at the synapses and in the dendrites. D1 receptor activation has been reported to enhance AMPA and *N*-methyl-D-aspartate (NMDA)-induced excitatory postsynaptic potentials (EPSPs), which may result in part from the enhancement of L-type Ca current in the dendrites (Cepeda et al. 1998; Galarraga et al. 1997; Surmeier et al. 1995; Umemiya and Raymond 1997). The enhancement of glutamatergic synaptic inputs, in particular through NMDA receptor effects, should work in concert with other mechanisms already discussed so as to increase the net inward current at intermediate potentials, thus creating a region of negative slope conductance and bistability.

Dopamine also plays a role in mediating long-term depression and long-term potentiation of the excitatory synapses converging on spiny neurons (Calabresi et al. 1997; Charpier and Deniau 1997; Kerr and Wickens 2001). This finding, in conjunction with the signaling properties of dopamine neurons while learning a task, led to the proposal that dopamine may be a training signal that mediates a form of reinforcement learning (Barto 1995; Houk et al. 1995; Montague et al. 1996). The proposed role of dopamine in learning and its role as a signal modulator are not mutually exclusive and may even complement each other. On one hand, dopamine-controlled modulation of the activity of spiny neurons can play the role of a reinforcement signal when included in an activity driven Hebbian learning rule for the modification of cortico-striatal synapses (Nakahara et al. 2002). A complementary mechanism is suggested by the observation that in the bistable regime, it is the input strength that selects the type of modulated response in rewarded trials. The demonstrated plasticity of cortico-striatal synapses (Calabresi et al. 1992, 1995; Charpier and Deniau 1997; Partridge et al. 2000; Reynolds and Wickens 2000) could then be utilized to adjust the excitatory input to spiny neurons to control the short-term modulation that occurs when dopamine levels are increased. This provides a mechanism for adaptable, learning-based signal processing in the striatum.

Functional implications of bistability

It follows from our model that D1-induced bistability increases the contrast of neural activity and can extend the duration of activity in the striatum. Other models have suggested that dopamine modulates the contrast of neural activity (Servan-Schreiber et al. 1990), but the temporal effect is a novel idea that may play an important role in information processing. Spiny neurons often have a longer duration response to stimuli that predictably precede reward (Hollerman et al. 1998; Kawagoe et al. 1998); although our model provides a cellular mechanism for enhanced duration, part of this effect could be attributed to network properties. The striatum is connected in a recurrent loop architecture with the rest of the basal ganglia, thalamus, and cortex (Alexander et al. 1986; Middleton and Strick 1997). The net positive feedback and additional nonlinearities provided by this type of network architecture can amplify and sustain modulatory effects, but there is still a need for a mechanism that initiates the modulation of the response to reward-predicting stimuli. The discharge properties of dopamine neurons and the neuromodulatory effect of dopamine on spiny neurons seem appropriate to fit this role. Dopamine-mediated modulation may serve as a gain mechanism that nonlinearly amplifies both the intensity and duration of the neural activity in the striatum to enhance the influence of this activity on downstream processing; this amplification, exported through thalamo-cortical pathways, may provide a mechanism for the preferential cortical encoding of salient information related to reward acquisition.

One major target of this efferent pathway is the frontal cortex (Middleton and Strick 2002). The basal ganglia and frontal cortex are part of a distributed system thought to be important for motor and cognitive functions (Graybiel 1997; Hikosaka et al. 2000; Houk and Wise 1995). Understanding how dopamine influences information processing within and between these areas may advance our understanding of the effects of dopamine on behavior. For instance, the sustained neural activity in the prefrontal cortex that subserves working memory functions (Fuster 1989; Goldman-Rakic 1987) is also dependent on reward expectation (Kobayashi et al. 2002; Tremblay and Schultz 2000; Watanabe 1996). In addition to direct dopaminergic actions in the cortex, dopamine-mediated modulation of spiny neurons that project to the frontal cortex via other basal ganglia nuclei and thalamus may contribute to the reward dependency of an initial activity, which is then maintained through recurrent connections. This sustained activity may provide a context for encoding subsequent information (Beiser and Houk 1998) and may impart reward dependence to neural responses related to events that occur after dopamine levels have returned to baseline, such as responses observed in prefrontal cortex and striatum in relation to memory, triggering cues, and delivery of reward (Hassani et al. 2001; Hollerman et al. 1998; Schultz et al. 1993; Watanabe 1998). The initial modulation of spiny neuron activity and its subsequent retention through sustained cortical activity may be a useful mechanism for preferentially encoding information related to acquiring rewards; this could be the neural basis for a mechanism by which phasic dopamine release in the striatum triggers the switching of attentional and behavioral resources toward salient events such as the presentation of a conditioned stimulus (Redgrave et al. 1999). This enhanced encoding of salient stimuli may thus underlie the improvement in latency, speed, and accuracy of saccades to rewarded targets as compared with saccades to unrewarded targets observed in subjects performing a memory-guided saccade task (Takikawa et al. 2002).

The functional effects of dopamine on striatal spiny neurons discussed here may complement those suggested by a recent model of dopaminergic action on cortical neurons (Durstewitz et al. 2000). These authors argue that dopamine stabilizes

activity in the prefrontal cortex by reducing the excitability of inactive units while enhancing the responsiveness of active units to current and subsequent excitatory inputs. Although there is experimental evidence (Maurice 2001) that conflicts with the cellular mechanisms on which their model is based, the processes responsible for the state-dependent modulation of excitability are functionally equivalent to increasing the L-type Ca current. The phenomenological description that emerges from these two models is thus similar: units in the hyperpolarized state are made less excitable by D1 receptor activation, whereas units in the depolarized state are made more excitable, which results in an effective increase of the contrast in neural activity. Our model demonstrates an additional feature: D1 receptor activation drives spiny neurons into a truly bistable regime where the emergence of hysteresis results in history-dependent temporal effects.

On a systems level, dopamine plays a significant role in the normal operation of the brain as evident in the severe cognitive and motor deficits apparent in patients suffering from Parkinson's disease, schizophrenia, and other dysfunctions associated with pathologies of the dopamine system. Yet on a cellular level, the effect of dopamine on the electrophysiology of neurons seems modest. Our model suggests that a small increase in the magnitude of both Kir2 and L-type Ca calcium currents elicited by D1 receptor activation suffices to switch the character of spiny neurons from bimodal to truly bistable, which not only modulates the frequency of neural responses but also introduces a state dependence and a temporal effect. Other models have shown that bistability enhances the functionality of cortical pyramidal cells (Camperi and Wang 1998), Purkinje cells (Yuen et al. 1995), and hippocampal pyramidal cells (Hahn and Durand 2001). We expect that the emergence of bistability in spiny neurons will significantly modulate signal propagation in the striatum. Our model indicates that dopamine is able to cause a temporary attenuation of spiny neuron responses to weak inputs while simultaneously enhancing spiny neuron responses to strong inputs. Modification of cortico-striatal synapses so as to preferentially enhance input components related to the most important features of a stimulus would ensure that this short-term modulation selectively enhances salient neural activity. Such selective enhancement in reward-related conditions could be a powerful computational mechanism for modulating the output of the striatum so as to provide a more informative efferent signal related to achieving reward.

To summarize, this paper presents a minimal cellular model of a spiny neuron that includes sufficient ionic and modulatory components so as to reproduce the prominent modulation of spiny neuron single-unit responses to conditioned stimuli. The model is based on a simplified yet biophysically grounded representation of relevant cellular mechanisms that operate in the 100 to 1,000 ms time range; it accounts for up- and down-state transitions of membrane potential, and describes a transition from bimodality to bistability triggered by dopamine release, D1 receptor activation, and the subsequent enhancement of key ion currents. When exposed to synaptic inputs, the model reveals a mechanism for both enhancement and depression of spiny neuron discharge in rewarded relative to unrewarded scenarios. The model incorporates information and tools from diverse areas of expertise: the biophysics of striatal spiny neurons, the mathematics of nonlinear dynamics, the modulation of ionic currents through D1 receptor activation and second-messenger pathways, the neuroanatomy of cortical-basal ganglionic networks, and single-unit neurophysiology in awake behaving monkeys. Findings from each of these disciplines have been combined here in an attempt to identify specific factors that contribute to the motivational components of neural activity currently being observed throughout the networks of the basal ganglia.

DISCLOSURES

A. J. Gruber acknowledges National Science Foundation support through its Integrative Graduate Education and Research Traineeship Grant on "Dynamics of Complex Systems in Science and Engineering". J. C. Houk acknowledges National Institutes of Health Grants MH-48185, NS-044393, and NS-044837. D. J. Surmeier acknowledges National Institutes of Health Grants NS-34696 and DA-12958.

REFERENCES

Akaike A, Ohno Y, Sasa M, and Takaori S. Excitatory and inhibitory effects of dopamine on neuronal activity of the caudate nucleus neurons in vitro. *Brain Res* 418: 262–272, 1987.

Alexander GE, DeLong MR, and Strick PL. Parallel organization of functionally segregated circuits linking basal ganglia and cortex. *Annu Rev Neurosci* 9: 357–381, 1986.

Bargas J, Howe A, Eberwine J, and Surmeier JD. Cellular and molecular characterization of Ca^{2+} currents in acutley isolated, adult rat neostraial neurons. *J Neurosci* 14: 6667–6686, 1994.

Barto AG. Adaptive critics and the basal ganglia. In: *Models of Information Processing in the Basal Ganglia*, edited by Houk JC, Davis JL, and Beiser DG. Cambridge, MA: MIT Press, 1995, p. 215–232.

Beiser DG and Houk JC. Model of cortical-basal ganglionic processing: encoding the serial order of senory events. *J Neurophysiol* 79: 3168–3188, 1998.

Bender CM and Orszag SA. Multiple-scale analysis. In: *Advanced Mathematical Methods for Scientists and Engineers.* New York: McGraw-Hill, 1978, p. 544–568.

Brown LL, Schneider JS, and Lidsky TI. Sensory and cognitive functions of the basal ganglia. *Curr Opin Neurobiol* 7: 157–163, 1997.

Calabresi P, Maj R, Pisani A, Mercuri NB, and Bernardi G. Long-term synaptic depression in the striatum: physiological and pharmacological characterization. *J Neurosci* 12: 4224–4233, 1992.

Calabresi P, Mercuri N, Stanzione P, Stefani A, and Bernardi G. Intracellular studies on the dopamine-induced firing inhibition of neostriatal neurons in vitro: evidence for D1 receptor involvement. *Neuroscience* 20: 757–771, 1987.

Calabresi P, Pisani A, Centonze D, and Bernardi G. Synaptic plasticity and physiological interactions between dopamine and glutamate in the striatum. *Neurosci Biobehav Rev* 21: 519–523, 1997.

Calabresi P, Pisani A, Mercuri NB, Gattoni G, Tolu M, and Bernardi G. Long-term changes of corticostriatal synaptic transmission: possible implication for motor memory. In: *Functions of the Cortico-Basal Ganglia Loop*, edited by Kimura M and Graybiel AM. Tokyo, Japan: Springer-Verlag, 1995, p. 89–103.

Camperi M and Wang XJ. A model of visuospatial working memory in prefrontal cortex: recurrent network and cellular bistability. *J Comput Neurosci* 5: 383–405, 1998.

Cepeda C, Colwell CS, Itri JN, Chandler SH, and Levine MS. Dopaminergic modulation of nmda-induced whole cell currents in neostriatal neurons in slices: contribution of calcium conductances. *J Neurophysiol* 79: 82–94, 1998.

Charpier S and Deniau JM. In vivo activity-dependent plasticity at cortico-striatal connections: evidence for physiological long-term potentiation. *Proc Natl Acad Sci USA* 94: 7036–7040, 1997.

Colby CL, Duhamel JR, and Goldberg ME. Visual, presaccadic, and cognitive activation of single neurons in monkey lateral intraparietal area. *J Neurophysiol* 76: 2841–2852, 1996.

Cooper DC and White FJ. L-type calcium channels modulate glutamate-driven bursting activity in the nucleus accumbens in vivo. *Brain Res* 880: 212–218, 2000.

Dugast C, Suaud-Chagny MF, and Gonon F. Continuous in vivo monitoring of evoked dopamine release in the rat nucleus accumbens by amperometry. *Neuroscience* 62: 647–654, 1994.

Durstewitz D, Seamans JK, and Sejnowski TJ. Dopamine-mediated stabilization of delay-period activity in a network model of prefrontal cortex. *J Neurophysiol* 83: 1733–1750, 2000.

Flores-Hernandez J, Hernandez S, Snyder GL, Yan Z, Fienberg AA, Moss SJ, Greengard P, and Surmeier DJ. D(1) dopamine receptor activation reduces $GABA_A$ receptor currents in neostriatal neurons through a pka/darpp-32/pp1 signaling cascade. *J Neurophysiol* 83: 2996–3004, 2000.

Funahashi S, Bruce CJ, and Goldman-Rakic PS. Visuospatial coding in primate prefrontal neurons revealed by oculomotor paradigms. *J Neurophysiol* 63: 814–831, 1990.

Fuster JM. *The Prefrontal Cortex: Anatomy, Physiology, and Neuropsychology of the Frontal Lobe.* New York: Raven, 1989.

Galarraga E, Hernandez-Lopez S, Reyes A, Barral J, and Bargas J. Dopamine facilitates striatal epsps through an L-type Ca^{2+} conductance. *Neuroreport* 8: 2183–2186, 1997.

Gerfen CR, Engber TM, Mahan LC, Susel Z, Chase TN, Monsma FJ, and Sibley DR. D_1 and D_2 dopamine receptors-regulated gene expression of striatonigral and striatopallidal neurons. *Science* 250: 1429–1432, 1990.

Goldman-Rakic PS. Circuitry of the frontal association cortex and its relevance to dementia. *Arch Gerontol Geriatr* 6: 299–309, 1987.

Gonon F. Prolonged and extrasynaptic excitatory action of dopamine mediated by D1 receptors in the rat striatum in vivo. *J Neurosci* 17: 5972–5978, 1997.

Grace AA. Phasic versus tonic dopamine release and the modulation of dopamine system responsivity: a hypothesis for the etiology of schizophrenia. *Neuroscience* 41: 1–24, 1991.

Graybiel AM. The basal ganglia and cognitive pattern generators. *Schizophr Bull* 23: 459–469, 1997.

Gruber AJ and Houk JC. A computational study of D1 induced modulation of medium spiny neuron response properties. *Soc Neurosci Abstr*, 26: 555.15, 2000.

Hahn PJ and Durand DM. Bistability dynamics in simulations of neural activity in high-extracellular-potassium conditions. *J Comput Neurosci* 11: 5–18, 2001.

Hassani OK, Cromwell HC, and Schultz W. Influence of expectation of different rewards on behavior-related neuronal activity in the striatum. *J Neurophysiol* 85: 2477–2489, 2001.

Hell JW, Westenbroek RE, Warner C, Ahlijanian MK, Prystay W, Gilbert MM, Snutch TP, and Catterall WA. Identification and differential subcellular localization of the neuronal class c and class d L-type calcium channel alpha 1 subunits. *J Cell Biol* 123: 949–962, 1993.

Hernandez SL, Bargas J, and Surmeier DJ. Activation of D1 dopamine receptors promotes up-state transitions in striatal medium spiny neurons. *Soc Neurosci Abstr* 28: 164.8, 2002.

Hernandez-Lopez S, Bargas J, Surmeier DJ, Reyes A, and Galarraga E. D1 receptor activation enhances evoked discharge in neostriatal medium spiny neurons by modulating an L-type Ca^{2+} conductance. *J Neurosci* 17: 3334–3342, 1997.

Hernandez-Lopez S, Tkatch T, Perez-Garci E, Galarraga E, Bargas J, Hamm H, and Surmeier DJ. D2 dopamine receptors in striatal medium spiny neurons reduce L-type Ca^{2+} currents and excitability via a novel PLCβ1-IP3-calcineurin-signaling cascade. *J Neurosci* 20: 8987–8995, 2000.

Herrera-Marschitz M, You ZB, Goiny M, Meana JJ, Silveira R, Godukhin OV, Chen Y, Espinoza S, Pettersson E, Loidl CF, Lubec G, Andersson K, Nylander I, Terenius L, and Ungerstedt U. On the origin of extracellular glutamate levels monitored in the basal ganglia of the rat by in vivo microdialysis. *J Neurochem* 66: 1726–1735, 1996.

Hikosaka O, Takikawa Y, and Kawagoe R. Role of the basal ganglia in the control of purposive saccadic eye movements. *Physiol Rev* 80: 953–978, 2000.

Hille B. *Ionic Channels of Excitable Membranes.* Sunderland, MA: Sinauer, 1992.

Hollerman JR, Tremblay L, and Schultz W. Influence of reward expectation on behavior-related neuronal activity in primate striatum. *J Neurophysiol* 80: 947–963, 1998.

Houk JC, Adams JL, and Barto AG. A model of how the basal ganglia generate and use neural signals that predict reinforcement. In: *Models of Information Processing in the Basal Ganglia*, edited by Houk JC, Davis JL, and Beiser DG. Cambridge, MA: MIT Press, 1995 p. 249–270.

Houk JC and Wise SP. Distributed modular architectures linking basal ganglia, cerebellum and cerebral cortex: their role in planning and controlling action. *Cereb Cortex* 5: 95–110, 1995.

Hu XT and Wang RY. Comparison of effects of d-1 and d-2 dopamine receptor agonists on neurons in the rat caudate putamen: an electrophysiological study. *J Neurosci* 8: 4340–4348, 1988.

Kawagoe R, Takikawa Y, and Hikosaka O. Expectation of reward modulates cognitive signals in the basal ganglia. *Nat Neurosci* 1: 411–416, 1998.

Kawagoe R, Takikawa Y, and Hikosaka O. Change in reward-predicting activity of monkey dopamine neurons: short term plasticity. *Soc Neurosci Abstr* 25: 470.12, 1999.

Kemp JM. The cortico-striate projection in the monkey. *Brain* 93: 525–546, 1970.

Kerr JN and Wickens JR. Dopamine d-1/d-5 receptor activation is required for long-term potentiation in the rat neostriatum in vitro. *J Neurophysiol* 85: 117–124, 2001.

Kitai ST. Monosynaptic inputs to caudate neurons identified by intracellular injection of horseradish peroxidase. *Brain Res* 109: 601–606, 1976.

Kitano K, Cateau H, Kaneda K, Nambu A, Takada M, and Fukai T. Two-state membrane potential transitions of striatal spiny neurons as evidenced by numerical simulations and electrophysiological recordings in awake monkeys. *J Neurosci* 22: 1–6, 2002.

Kiyatkin EA and Rebec GV. Dopaminergic modulation of glutamate-induced excitations of neurons in the neostriatum and nucleus accumbens of awake, unrestrained rats. *J Neurophysiol* 75: 142–153, 1996.

Kiyatkin EA and Rebec GV. Striatal neuronal activity and responsiveness to dopamine and glutamate after selective blockade of D1 and D2 dopamine receptors in freely moving rats. *J Neurosci* 19: 3594–3609, 1999.

Kobayashi S, Lauwereyns J, Koizumi M, Sakagami M, and Hikosaka O. Influence of reward expectation on visuospatial processing in macaque lateral prefrontal cortex. *J Neurophysiol* 87: 1488–1498, 2002.

Ljungberg T, Apicella P, and Schultz W. Responses of monkey midbrain dopamine neurons during delayed alternation performance. *Brain Res* 567: 337–341, 1991.

Ljungberg T, Apicella P, and Schultz W. Responses of monkey dopamine neurons during learning of behavioral reactions. *J Neurophysiol* 67: 145–163, 1992.

Matsumoto N, Hanakawa T, Maki S, Graybiel AM, and Kimura M. Nigrostriatal dopamine system in learning to perform sequential motor tasks in a predictive manner. *J Neurophysiol* 82: 978–998, 1999.

Maurice N. D1/D5 dopamine receptor activation differentially modulates rapidly inactivating and persistent sodium currents in prefrontal cortex pyramidal neurons. *J Neurosci* 21: 2268–2277, 2001.

Maurice N, Tkatch T, Burnell K, and Surmeier DJ. D2 dopamine receptors decrease rapidly inactivating and persistent sodium currents via a PLC/pkc cascade in mouse striatal medium spiny neurons. *Soc Neurosci Abstr* 27: 67.9, 2001.

Mermelstein PG, Song W-J, Tkatch T, Yan Z, and Surmeier DJ. Inwardly rectifying potassium currents are correlated with irk subunit expression in rat nucleus accumbens medium spiny neurons. *J Neurosci* 18: 6650–6661, 1998.

Middleton FA and Strick PL. New concepts about the organization of basal ganglia output. *Adv Neurol* 74: 57–68, 1997.

Middleton FA and Strick PL. Basal-ganglia "projections" to the prefrontal cortex of the primate. *Cereb Cortex* 12: 926–935, 2002.

Mirenowicz J and Schultz W. Importance of unpredictability for reward responses in primate dopamine neurons. *J Neurophysiol* 72: 1024–1027, 1994.

Mirenowicz J and Schultz W. Preferential activation of midbrain dopamine neurons by appetitive rather than aversive stimuli. *Nature* 379: 449–451, 1996.

Montague PR, Dayan P, and Sejnowski TJ. A framework for mesencephalic dopamine systems based on predictive hebbian learning. *J Neurosci* 16: 1936–1947, 1996.

Nakahara H, Amari S, and Hikosaka O. Self-organization in the basal ganglia with modulation of reinforcement signals. *Neural Comp* 14: 819–844, 2002.

Nicola SM, Surmeier J, and Malenka RC. Dopaminergic modulation of neuronal excitability in the striatum and nucleus accumbens. *Annu Rev Neurosci* 23: 185–215, 2000.

Nisenbaum ES and Wilson CJ. Potassium currents responsible for inward and outward rectification in rat neostriatal spiny projection neurons. *J Neurosci* 15: 4449–4463, 1995.

Nisenbaum ES, Wilson CJ, Foehring RC, and Surmeier DJ. Isolation and characterization of a persistent potassium current in neostriatal neurons. *J Neurophysiol* 76: 1180–1194, 1996.

Olson PA and Surmeier DJ. M1 muscarinic receptors modulate Cav1.3 L-type calcium channels in medium spiny neurons in the nucleus accumbens shell. *Soc Neurosci Abstr* 28: 164.6, 2002.

Pacheco-Cano MT, Bargas J, and Hernández-López S. Inhibitory action of dopamine involves a subthreshold c_s^+-sensitive conductance in neostriatal neurons. *Exp Brain Res* 110: 205–211, 1996.

Partridge JG, Tang KC, and Lovinger DM. Regional and postnatal heterogeneity of activity-dependent long-term changes in synaptic efficacy in the dorsal striatum. *J Neurophysiol* 84: 1422–1429, 2000.

Pierce RC and Rebec GV. Iontophoresis in the neostriatum of awake, unrestrained rats: differential effects of dopamine, glutamate and ascorbate on motor- and nonmotor-related neurons. *Neuroscience* 67: 313–324, 1995.

Rebec GV. Real-time assessments of dopamine function during behavior: single-unit recording, iontophoresis, and fast-scan cyclic voltammetry in awake, unrestrained rats. *Alcohol Clin Exp Res* 22: 32–40, 1998.

Redgrave P, Prescott TJ, and Gurney K. Is the short-latency dopamine response too short to signal reward error? *Trends Neurosci* 22: 146–151, 1999.

Reynolds JN and Wickens JR. Substantia nigra dopamine regulates synaptic plasticity and membrane potential fluctuations in the rat neostriatum, in vivo. *Neuroscience* 99: 199–203, 2000.

Richfield EK, Penney JB, and Young AB. Anatomical and affinity state comparisons between dopamine D1 and D2 receptors in the rat central nervous system. *Neuroscience* 30: 767–777, 1989.

Rinzel J and Ermentrout GB. Analysis of neural excitability and oscillations. In: *Methods in Neuronal Modeling*, edited by Koch C and Segev I. Cambridge, MA: MIT Press, 1989, p. 135–169.

Schultz W, Apicella P, and Ljungberg T. Responses of monkey dopamine neurons to reward and conditioned stimuli during successive steps of learning a delayed response task. *J Neurosci* 13: 900–913, 1993.

Schultz W, Apicella P, Romo R, and Scarnati E. Context-dependent activity in primate striatum reflecting past and future behavioral events. In: *Models of Information Processing in the Basal Ganglia*, edited by Houk JC, Davis JL, and Beiser DG. Cambridge, MA: MIT Press, 1995, p. 11–27.

Schultz W. Predictive reward signal of dopamine neurons. *J Neurophysiol* 80: 1–27, 1998.

Selemon LD. Longitudinal topography and interdigitation of corticostriatal projections in the rhesus monkey. *J Neurosci* 5: 776–794, 1985.

Servan-Schreiber D, Printz H, and Cohen JD. A network model of catecholamine effects: gain, signal-to-noise ratio, and behavior. *Science* 249: 892–895, 1990.

Song WJ and Surmeier DJ. Voltage-dependent facilitation of calcium channels in rat neostriatal neurons. *J Neurophysiol* 76: 2290–2306, 1996.

Stern EA, Kincaid AC, and Wilson CJ. Spontaneous subthreshold membrane potential fluctuations and action potential variability of rat corticostriatal and striatal neurons in vivo. *J Neurophysiol* 77: 1697–1715, 1997.

Surmeier DJ, Bargas J, Hemmings HC, Jr, Nairn AC, and Greengard P. Modulation of calcium currents by a D_1 dopaminergic protein kinase/phosphatase cascade in rat neostriatal neurons. *Neuron* 14: 385–397, 1995.

Surmeier DJ, Eberwine J, Wilson CJ, Cao Y, Stefani A, and Kitai ST. Dopamine receptor subtypes colocalize in rat striatonigral neurons. *Proc Natl Acad Sci USA* 89: 10178–10182, 1992a.

Surmeier DJ and Kitai ST. D1 and D2 dopamine receptor modulaiton of sodium and potassium currents in rat neostriatal neurons. In: *Progress in Brain Research* edited by Arbuthnott GW and Emson PC. Amsterdam: Elsevier, 1993, vol. 99, p. 309–324.

Surmeier DJ, Song W-J, and Yan Z. Coordinated expression of dopamine receptors in neostriatal medium spiny neurons. *J Neurosci* 16: 6579–6591, 1996.

Surmeier DJ, Stefani A, Foehring RC, and Kitai ST. Developmental regulation of a slowly-inactivating potassium conductance in rat neostriatal neurons. *Neurosci Lett* 122: 41–46, 1991.

Surmeier DJ, Xu ZC, Wilson CJ, Stefani A, and Kitai ST. Grafted neostriatal neurons express a late-developing transient potassium current. *Neuroscience* 48: 849–856, 1992b.

Takikawa Y, Kawagoe R, Itoh H, Nakahara H, and Hikosaka O. Modulation of saccadic eye movements by predicted reward outcome. *Exp Brain Res* 142: 284–291, 2002.

Tremblay L and Schultz W. Reward-related neuronal activity during go-nogo task performance in primate orbitofrontal cortex. *J Neurophysiol* 83: 1864–1876, 2000.

Umemiya M and Raymond LA. Dopaminergic modulation of excitatory postsynaptic currents in rat neostriatal neurons. *J Neurophysiol* 78: 1248–1255, 1997.

Vilchis C, Bargas J, Ayala GX, Galvan E, and Galarraga E. Ca^{2+} channels that activate Ca^{2+}-dependent K^+ currents in neostriatal neurons. *Neuroscience* 95: 745–752, 2000.

Watanabe M. Reward expectancy in primate prefrontal neurons. *Nature* 382: 629–632, 1996.

Watanabe M. Cognitive and motivational operations in primate prefrontal neurons. *Rev Neurosci* 9: 225–241, 1998.

Watanabe M, Hikosaka K, Sakagami M, and Shirakawa S. Coding and monitoring of motivational context in the primate prefrontal cortex. *J Neurosci* 22: 2391–2400, 2002.

Wickens JR and Arbuthnott GW. The corticostriatal system on computer simulation: an intermediate mechanism for sequencing of actions. In: *Progress in Brain Research, Chemical Signalling in the Basal Ganglia*, edited by Arbuthnott GW and Emson PC. Amsterdam: Elsevier, 1993, vol. 99, p. 325–339.

Williams GV and Millar J. Concentration-dependent actions of stimulated dopamine release on neuronal activity in rat striatum. *Neuroscience* 39: 1–16, 1990.

Wilson CJ and Groves PM. Spontaneous firing patterns of identified spiny neurons in the rat neostriatum. *Brain Res* 220: 67–80, 1981.

Wilson CJ. Basal ganglia. In: *The Synaptic Organization of the Brain*, edited by Shepherd GM. New York: Oxford Univ. Press, 1990, p. 279–316.

Wilson CJ. The generation of natural firing patterns in neostriatal neurons. In: *Progress in Brain Research, Chemical Signalling in the Basal Ganglia*, edited by Arbuthnott GW and Emson PC. Amsterdam: Elsevier, 1993, vol. 99, p. 277–297.

Wilson CJ and Kawaguchi Y. The origins of two-state spontaneous membrane potential fluctuations of neostriatal spiny neurons. *J Neurosci* 16: 2397–2410, 1996.

Yuen GL, Hockberger PE, and Houk JC. Bistability in cerebellar purkinje cell dendrites modelled with high-threshold calcium and delayed-rectifier potassium channels. *Biol Cybern* 73: 375–388, 1995.